THE JOURNAL OF BIOLOGICAL CHEMISTRY VOL. 290, NO. 10, pp. 5960–5978, March 6, 2015
© 2015 by The American Society for Biochemistry and Molecular Biology, Inc. Published in the U.S.A.

Targeting Interleukin-2-inducible T-cell Kinase (ITK) and Resting Lymphocyte Kinase (RLK) Using a Novel Covalent Inhibitor PRN694[S]

Received for publication, September 26, 2014, and in revised form, January 13, 2015 Published, JBC Papers in Press, January 15, 2015, DOI 10.1074/jbc.M114.614891

Yiming Zhong[‡], Shuai Dong[§], Ethan Strattan[‡], Li Ren[‡], Jonathan P. Butchar[‡], Kelsey Thornton[‡], Anjali Mishra[‡], Pierluigi Porcu[‡], J. Michael Bradshaw[¶], Angelina Bisconte[¶], Timothy D. Owens[¶], Erik Verner[¶], Ken A. Brameld[¶], Jens Oliver Funk[¶], Ronald J. Hill[¶1], Amy J. Johnson[‡2], and Jason A. Dubovsky[‡2,3]

From the [‡]Division of Hematology, College of Medicine, Ohio State University, Columbus, Ohio 43210, the [§]Division of Pharmaceutics and Pharmaceutical Chemistry, College of Pharmacy, Ohio State University, Columbus, Ohio 43210, and [¶]Principia Biopharma, South San Francisco, California 94080

Background: ITK and RLK are unique to effector lymphocytes and critical for immune activation.
Results: A novel selective covalent ITK/RLK inhibitor called PRN694 was discovered, which blocks T-cell and NK cell activation.
Conclusion: PRN694 provides an effective tool to elucidate the roles of ITK and RLK in immune cell signaling.
Significance: PRN694 could be an effective therapy for T-cell- or NK cell-driven autoimmune, inflammatory, and malignant diseases.

Interleukin-2-inducible T-cell kinase (ITK) and resting lymphocyte kinase (RLK or TXK) are essential mediators of intracellular signaling in both normal and neoplastic T-cells and natural killer (NK) cells. Thus, ITK and RLK inhibitors have therapeutic potential in a number of human autoimmune, inflammatory, and malignant diseases. Here we describe a novel ITK/RLK inhibitor, PRN694, which covalently binds to cysteine residues 442 of ITK and 350 of RLK and blocks kinase activity. Molecular modeling was utilized to design molecules that interact with cysteine while binding to the ATP binding site in the kinase domain. PRN694 exhibits extended target residence time on ITK and RLK and is highly selective for a subset of the TEC kinase family. *In vitro* cellular assays confirm that PRN694 prevents T-cell receptor- and Fc receptor-induced cellular and molecular activation, inhibits T-cell receptor-induced T-cell proliferation, and blocks proinflammatory cytokine release as well as activation of Th17 cells. *Ex vivo* assays demonstrate inhibitory activity against T-cell prolymphocytic leukemia cells, and *in vivo* assays demonstrate durable pharmacodynamic effects on ITK, which reduces an oxazolone-induced delayed type hypersensitivity reaction. These data indicate that PRN694 is a highly selective and potent covalent inhibitor of ITK and RLK, and its extended target residence time enables durable attenuation of effector cells *in vitro* and *in vivo*. The results from this study highlight potential applications of this dual inhibitor for the treatment of T-cell- or NK cell-mediated inflammatory, autoimmune, and malignant diseases.

IL-2-inducible T-cell kinase (ITK)[4] and resting lymphocyte kinase (RLK; also known as TXK) are members of the TEC family of non-receptor tyrosine kinases that play important roles in signal transduction in T-cells and natural killer (NK) cells (1–3). ITK and RLK facilitate a range of downstream signaling from T-cell and NK cell surface receptors, tyrosine kinases, and integrins, including the T-cell receptor (TCR) and Fc receptor (FcR) (1, 4, 5). Upon surface receptor engagement, ITK mediates signaling by activating phospholipase Cγ1 (PLCγ1), leading to the downstream activation of nuclear factor of activated T-cells (NFAT), nuclear factor κB (NFκB), and mitogen-activated protein kinase (MAPK) pathways (6). ITK knock-out ($ITK^{-/-}$) mice demonstrate defects in Th2 and Th17 differentiation and function (7). The Th2 deficiency initiated interest in ITK as a therapeutic target in asthma, because $Itk^{-/-}$ mice are resistant to ovalbumin-induced asthma (8). More recently, attention has shifted to autoimmune disease because of the effects of ITK deletion on Th17 function and the concomitant increase in regulatory T-cell (Treg) numbers and function (9). The clinical target validation of IL-17 in psoriasis and psoriatic arthritis adds additional support to the notion that ITK could be a relevant therapeutic target in these diseases (10). In addition, interest remains high in other Th17-driven autoimmune diseases, such as multiple sclerosis and inflammatory bowel disease (11).

The signaling of RLK is less clear. Its unique N-terminal structure, which lacks the pleckstrin homology domain present in other TEC kinases, renders it free of modulation by phos-

[S] This article contains supplemental Table 1.

[1] To whom correspondence may be addressed: Principia Biopharma, 400 E. Jamie Ct., Suite 302, South San Francisco, CA 94080. Tel.: 650-416-7717; E-mail: ron.hill@principiabio.com.
[2] Both authors contributed equally to this work.
[3] To whom correspondence may be addressed: Dept. of Internal Medicine, Division of Hematology, Ohio State University, OSUCCC Bldg., Rm. 479, 410 W. 12th Avenue., Columbus, OH 43210. Tel.: 614-688-8557; E-mail: jason.dubovsky@nationwidechildrens.org.

[4] The abbreviations used are: ITK, interleukin-2-inducible T-cell kinase; RLK, resting lymphocyte kinase; NK, natural killer; TCR, T cell receptor; FcR, Fc receptor; PLCγ1, phospholipase Cγ1; NFAT, nuclear factor of activated T-cells; DTH, delayed type hypersensitivity; PBMC, peripheral blood mononuclear cell; CFSE, carboxyfluorescein succinimidyl ester; BisTris, 2-[bis(2-hydroxyethyl)amino]-2-(hydroxymethyl)propane-1,3-diol; DNP, dinitrophenyl; BTK, Bruton's tyrosine kinase; T-PLL, T-cell prolymphocytic leukemia.

phoinositide-3 kinase activity (12). Deletion of RLK alone has few functional consequences, but deletion of RLK in combination with ITK appears to be important in Th1 cells, where it is preferentially expressed. In addition, the deletion of ITK and RLK has a marked effect on Th17 differentiation and IL-17 production (13). In some settings, it appears that ITK and RLK are redundant signaling molecules because overexpression of RLK in $ITK^{-/-}$ mice rescues the Th2 response in a model of asthma (14). Importantly, ITK and RLK are aberrantly overexpressed and activated in T-cell malignancies as well as inflammatory and autoimmune diseases, making these proteins particularly attractive therapeutic targets in these disorders (4, 15–17).

To date, no small molecule inhibitors specifically targeting ITK or RLK have progressed past preclinical studies. Conventional approaches to developing reversible competitive inhibitors have been hampered by limited potency and/or selectivity, although efforts continue to be made (18–22). A recent study utilizing non-competitive binding to an allosteric site of ITK has yielded a compound with high selectivity; however, the absorption, distribution, metabolism, and excretion and physicochemical optimization to produce the extended pharmacokinetics required for reversible compounds has not been completed (23). Because RLK is thought to compensate for ITK in a number of T-cell and NK cell subsets, development of a dual ITK/RLK inhibitor would be advantageous to effectively block TEC kinase-driven activation of these cells (12).

Covalent targeting of cysteine residues within the ATP binding pocket is an effective way to obtain highly potent and selective kinase inhibitors with long target residence time (24, 25). Ibrutinib, for instance, irreversibly binds cysteine 481 in BTK and cysteine 442 in ITK, leading to a blockade of signaling downstream of the B-cell receptor and TCR, respectively. Ibrutinib has demonstrated clinical safety and activity against B-cell malignancies, including mantle cell lymphoma and chronic lymphocytic leukemia (26–28). All five mammalian TEC kinases have a similar domain organization, including a cysteine-containing kinase domain (4). Herein we describe PRN694, which was developed to irreversibly inhibit ITK and RLK by forming a putative covalent bond with Cys-442 or Cys-350, respectively. We show that this results in *in vivo* efficacy without the need for an extended plasma half-life. *In vitro* kinase assays show that PRN694 has potency and selectivity for ITK and RLK. This selectivity is validated in Jurkat T-cells with mutated ITK or overexpressed RLK. We further demonstrate that PRN694 prevents TCR- or FcR-induced cellular and molecular activation, inhibits TCR-induced T-cell proliferation without direct cytotoxicity, and blocks proinflammatory cytokine release. Finally, *in vivo* experiments demonstrate the pharmacokinetics and pharmacodynamics of PRN694 and show that it attenuates a delayed type hypersensitivity (DTH) reaction in a well established murine model system. These results indicate promising clinical applicability of this ITK/RLK dual inhibitor for the treatments of T-cell or NK cell malignancies as well as inflammatory and autoimmune diseases, such as psoriasis, psoriatic arthritis, rheumatoid arthritis, multiple sclerosis, and irritable bowel disease.

EXPERIMENTAL PROCEDURES

Patient Samples—T-cells and peripheral blood mononuclear cells (PBMCs) were obtained from normal donors or patients diagnosed with T-cell leukemia. Deidentified specimens were obtained from the Ohio State University Comprehensive Cancer Center Leukemia Tissue Bank. All subjects gave written, informed consent for their blood products to be used for research under an Institutional Review Board-approved protocol in accordance with the Declaration of Helsinki.

Cell Separation, Culture Conditions, and Inhibitor Treatment—Primary CD3, CD4, and/or CD8 T-cells were isolated using negative selection (EasySep, StemCell Technologies, Vancouver, Canada) or magnetic separation (MACS Human $CD17^+$ microbeads, Miltenyi, Auburn, CA) according to the manufacturer's protocol. Primary NK cells were isolated using RosetteSep human NK cell enrichment mixture (StemCell Technologies) according to the manufacturer's protocol. Cells were cultured *in vitro* at 37 °C and 5% CO_2 using RPMI 1640 with 10% fetal calf serum. Cells were pretreated for 30 min with PRN694 or other inhibitors and then washed two times. T-cells were then stimulated for 6 h with 1 μg/ml soluble anti-CD3 (eBiosciences, San Diego, CA) for CD69 activation, which was detected by flow cytometry, or 45 min with plate-bound anti-CD3 (10 μg/ml plating concentration) and soluble anti-CD28 (1 μg/ml) (eBiosciences) for downstream signal analysis by immunoblotting. NK cells were stimulated for 6 h with plate-bound anti-CD52 (alemtuzumab) for CD107a/b (BD Biosciences) activation, detected by flow cytometry, or for 45 min for downstream signal analysis by immunoblotting. Nuclear and cytoplasmic lysates (NE-PER kit, Thermo, Rockford, IL) or whole cell lysates were collected for immunoblotting.

Reverse Transcription-PCR (RT-PCR)—Total RNA was prepared from pelleted cells using the Total RNA Purification Plus kit (Norgen Biotek Corp.). Quantitative RT-PCRs were conducted using the Taqman one-step RT-PCR kit (Invitrogen) with transcript-specific Taqman primers (Itk, Hs00950634_m1; Rlk, Hs00177433_m1; Gapdh, Hs02758991_g1). Quantitative RT-PCR experiments were analyzed using the MyiQ software package. After confirming a single melt curve peak, *CT* values for GAPDH were compared with *CT* values for the transcript of interest using the Pfaffl method (29).

Flow Cytometry—Flow cytometric analysis was performed using fluorochrome-labeled monoclonal antibodies (mAbs; anti-CD4, -CD8, -CD19, -CD17a, -CD107a, -CD107b, -IL-4, -IFNγ) as well as annexin V-FITC and propidium iodide (BD Biosciences). Intracellular staining was conducted according the manufacturer's protocol (BD Biosciences). Samples were washed once prior to analysis. Flow cytometric data were analyzed with FlowJo or Kaluza software (Tree Star (Ashland, OR) and Beckman Coulter (Indianapolis, IN), respectively) on a minimum of 30,000 collected events. Phosphoflow analysis of pPLCγ1 was conducted as described previously (28).

Cytometric Bead Assay—A cytometric bead assay (BD Biosciences) was conducted according to the manufacturer's published protocol using cellular supernatant from three replicate experiments as described previously (28).

Carboxyfluorescein Succinimidyl Ester (CFSE) Proliferation Assay—CFSE cell proliferation assays were performed as described previously (30). Briefly, isolated CD3 T-cells were resuspended in prewarmed PBS at 1×10^6 cells/ml, mixed with 1 μM CFSE, and incubated at 37 °C for 10 min. After staining and subsequent washing, cells were cultured at 37 °C for 6 days, and proliferation was measured via CFSE flow cytometry.

Delayed Type Hypersensitivity—Mice were randomized by weight and sensitized with aliquots of 150 μl of 5% oxazolone (Sigma catalog no. EO) in 3 parts ethanol and 1 part acetone on their shaved abdomens. Seven days after the sensitization, the mice were challenged with 10 μl of 3% oxazolone on the front and back of the right ears. The left ears were treated with the ethanol/acetone mixture. One hour prior to the challenge, the animals received either vehicle control (5% ethanol, 95% Captex 355 NP/EF, intraperitoneal injection at 5 ml/kg), 20 mg/kg PRN694 in 5% ethanol, 95% Captex (intraperitoneal injection at 5 ml/kg), or 0.5 mg/kg dexamethasone (intraperitoneal injection at 5 ml/kg). A control group of animals received no oxazolone or drug treatment. Twenty-four hours after the oxazolone challenge, the mice were sacrificed, and a 7-mm disc was punched out of each ear and weighed to measure edema. The DTH studies were performed at Bolder Biopath (Boulder, CO).

Antibody-dependent Cellular Cytotoxicity (ADCC)—ADCC was tested as described previously using purified human PBMCs for the effector cell population (31). Briefly, 50-μl tripling dilutions from 1 to 0.005 μM PRN694 or PRN403 (2× final concentration) were preincubated with 50 μl of PBMCs (All Cells, catalog no. CUS-PBMC-006) at room temperature for 1 h. Target cells (10^5 Jeko-1 cells in 50 μl) were preincubated with 4 μg/ml anti-CD20 antibody (Eureka Therapeutics) at 37 °C for 30 min. Compound-treated PBMCs (5×10^6 cells in a 100-μl total volume) were added to target cells at an effector/target ratio of 25:1 and incubated for 16 h. After incubation, the cells were pelleted by centrifugation, and the supernatant was assayed for lactate dehydrogenase release (Cytotox 96 nonradiocytotoxicity, Promega, catalog no. G1780) as a measure of cell lysis. Specific lysis was calculated as ((experimental release − spontaneous release)/maximum release − spontaneous release)) × 100. The ADCC assays were performed at Eureka Therapeutics (Emeryville, CA).

Immunoblot—Experiments were conducted using conventional methodology as described previously (32). Blotting was conducted using pPLCγ1 2821, PLCγ1 2822, NFAT1 4389S, ITK 2380S, JUNB 3746S, and pIκBα 9246L antibodies (Cell Signaling Technologies, Danvers, MA) or IκBα sc-371, lamin B sc-6216, and actin sc-1615 antibodies (Santa Cruz Biotechnology, Inc.). Densitometry analysis was conducted using ImageJ analysis software (National Institutes of Health). Raw density was normalized to the intensity of vehicle-treated stimulated cells.

Calcium Flux Assays—Experiments were conducted as described previously (28).

Chromium Release Cytotoxicity Assays—Ficoll gradient-isolated PBMC targets obtained from healthy donors were incubated with ^{51}Cr for 1 h at 100 μCi/10^6 cells and subsequently washed. RosetteSep-isolated CD8 T-cells were treated with 0.5 μM PRN694 or DMSO and then added to target cells at an effector/target ratio of 50:1 for 4 h. Afterward, supernatant was harvested, and γ radiation was counted using a PerkinElmer Wizard 2 automatic γ counter. The percentage of cytotoxicity was calculated from triplicate samples using the equation, $(X - \text{Min})/(\text{Max} - \text{Min}) = \%$ lysis.

In Vitro Kinase Assay—Inhibitor potency in ITK or RLK enzymatic assays was determined using the microfluidics-based LabChip 3000 drug discovery system (Caliper Life Sciences). Twelve concentrations of inhibitor were first preincubated with recombinant ITK or RLK. Enzyme, inhibitor, peptide substrate, and cofactors (ATP and Mg^{2+}) were then combined and incubated at 25 °C. The final assay reaction mixture contained a buffer of 100 mM HEPES, pH 7.5, 0.1% BSA, 0.01% Triton X-100, 1 mM DTT, 10 mM $MgCl_2$, 10 μM sodium orthovanadate, 10 μM β-glycerophosphate, 16 μM ATP, and 1% DMSO. The ATP concentration was 10 nM for ITK and 100 nM for RLK. At the end of the incubation, the reaction was quenched by the addition of an EDTA-containing buffer. Negative control samples (containing no inhibitor) and positive control samples (tested in the presence of 20 mM EDTA) were simultaneously evaluated in order to calculate the percentage inhibition at each compound concentration. The IC_{50} values were determined by fitting the inhibition curves (percentage inhibition *versus* inhibitor concentration) using a 4-parameter sigmoidal dose-response model (XLfit4 software, IBDS (Alameda, CA)). The determination of enzymatic IC_{50} values for BLK, BMX, BTK, EGFR, ERB-B2, ERB-B4, JAK3, MKK7, and TEC was performed as described above except that the concentration of kinase, the peptide substrate, and the ATP concentration were optimized for each kinase. Similarly, the broader screen of 250 kinases was performed under optimized ATP concentration conditions. Determination of k_{inact}/K_i for ITK and RLK was performed by acquiring real-time peptide phosphorylation progress curves at 12 concentrations of PRN694 and subsequently fitting the rate of enzyme inactivation as a function of inhibitor concentration to establish k_{inact}/K_i. Enzymatic IC_{50} assays as well as single concentration screening assays were performed by Nanosyn, Inc. (Santa Clara, CA).

In Silico Molecular Design—All molecular modeling was performed with the Molecular Operating Environment (MOE) software package (Chemical Computing Group Inc., Montreal, Canada). Protein crystal structures 3QGY, 3MIY, 4HCU, and 3V8T were downloaded from the Protein Data Bank and prepared for modeling with the "Structure Preparation" module. The MMFF94x force field and the R-field solvation model were used for all energy minimization calculations. Designed ligands were manually docked into the ATP binding site and energy-minimized to release any molecular strain. Conformational models of the covalently bonded ligand were generated using a low mode conformational analysis followed by energy minimization. Diverse molecular designs were evaluated and scored based upon a visual analysis of the final docked conformation.

Determination of ITK Occupancy in Vivo—Mouse thymus tissue was removed at the time of sacrifice, and a single cell suspension of thymocytes was prepared. Thymocytes were treated with a 1 μM concentration of an irreversible BODIPY-labeled ITK-selective probe (synthesized by Principia Biopharma) that labels unbound ITK. Cells were washed and lysed in lysis buffer (Cell Lytic M, Sigma catalog no. C2978) supple-

mented with protease inhibitor mixture (Pierce Protease and phosphatase inhibitor, Thermo Scientific catalog no. 88669). Each sample was separated on a 4–12% BisTris SDS-polyacrylamide gel (Novex®, Invitrogen) to determine occupancy of ITK. Gels were scanned for probe binding on a Typhoon image scanner (GE Healthcare) using the Fluorescein 526 emission filter, photomultiplier tube at 800 V, and green laser. To evaluate the total ITK present in each sample, gels were transferred to nitrocellulose using an iBlot system (Invitrogen). Membranes were probed overnight with anti-ITK (BD Biosciences catalog no. 51-6979 1N), detected with goat anti-mouse antibody conjugated to AlexaFluor 647 (Invitrogen, catalog no. A21236, 1:1000) and scanned on a Typhoon 9410 or 8600 variable mode imager (GE Healthcare) with an emission filter of Cy5 670 BP30 and red laser. Band intensities were quantified using ImageQuant software (GE Healthcare). For each sample, the fluorescent signal was normalized for total ITK, and the percentage of occupancy was calculated by subtracting the normalized ratio from 100%.

Determination of PRN694 Off-rate with Recombinant ITK—Recombinant ITK at a final concentration of 0.5 μM in 50 mM Hepes, pH 7.5, 10 mM $MgCl_2$, 0.01% Triton X-100, and 1 mM EGTA (His_6-labeled, Millipore catalog no. 13-660) were combined with 1.5 μM PRN694 or BMS-509744 for 90 min to facilitate binding. The mixture was then diluted 50-fold to initiate dissociating of the ligand from the enzyme, and 10 μl was transferred to a Greiner 384-well black plate. Europium-coupled anti-His_6 antibody (PerkinElmer Life Sciences ADO205) was added to each well and incubated for 5 min, followed by the addition of an ITK binding fluorescent tracer (Tracer 236, Invitrogen PV5592). The tracer binds to ITK as a function of ligand dissociation, and binding is detected by time-resolved FRET between the europium-coupled antibody and the AlexaFluor 647-labeled tracer 236 on a PerkinElmer Envision® model 2101 plate reader. Time points acquired were 0.25, 1, 3, 6, and 24 h.

Macrophage, Dendritic Cell, and Mast Cell Activation—Human $CD14^+$ peripheral blood monocytes were magnetically isolated (Miltenyi) and incubated on plates for 7 days either with 20 ng/ml recombinant human M-CSF (R&D Systems, Minneapolis, MN) to generate monocyte-derived macrophages or with 20 ng/ml each of recombinant human GM-CSF and recombinant human IL-4 (R&D Systems) to generate monocyte-derived dendritic cells. Factors were re-added on days 3 and 5, and cells were harvested for use on day 7. To test FcγR-mediated cytokine production, cells were pretreated with 0.5 μM PRN694 or DMSO at 37 °C for 30 min. Following two washes in PBS, cells were plated at 1×10^6 cells/ml in 96-well plates (2×10^5 cells/well) precoated with or without 10 μg/ml human IgG (Jackson Immunoresearch). After 24 h, cleared supernatants were collected and assayed by ELISA for TNFα and IL-12 (R&D Systems).

For mast cell assays 2×10^5 RBL-2H3 cells (ATCC) were sensitized with 1 μg/ml anti-dinitrophenyl (DNP) IgE for 3 h. After three washes to remove excess antibody, cells were pretreated with 0.5 μM PRN694 or DMSO for 30 min, washed, and subsequently stimulated with 1 μg/ml DNP for 30 min. Histamine production was measured by ELISA (Genway Biotech, Inc., San Diego, CA) according to the manufacturer's directions.

Statistics—Unless otherwise noted, a two-tailed student's *t* test was used for normal data at equal variance. Significance was considered for $p < 0.05$. All analyses were performed using SAS/STAT software, version 9.2 (SAS Institute Inc., Cary, NC).

RESULTS

Structure, Potency, and Specificity of PRN694—We discovered highly selective ITK/RLK inhibitors using a combination of covalent targeting technology and structure-based design. Of primary importance was the need to identify a hinge-binding molecular scaffold and compatible linker chemistry to covalently bond to ITK Cys-442. A superposition of all of the available x-ray crystal structures of ITK in complex with small molecule inhibitors was undertaken. Upon visual inspection, several structures deposited in the Protein Data Bank (entries 3QGY, 3MIY, 4HCU, and 3V8T) presented suitable vectors to target Cys-442. Molecular modeling and a synthetic feasibility assessment led to the prioritization of several small focused compound libraries. The structure-based medicinal chemistry optimization of one such library culminated in the identification of PRN694, a potent irreversible inhibitor of ITK and RLK (Fig. 1, *A–C*). The biochemical occupancy of PRN694 on recombinant ITK did not decrease over time (Fig. 1*C*), which is consistent with its formation of an irreversible covalent bond with the target. This is in contrast to the completely reversible molecule BMS-509744, which forms no covalent interaction with ITK and quickly dissociates from the target. In similar experiments, the occupancy of PRN694 on recombinant RLK was 85 ± 4% after 24 h, also consistent with formation of an irreversible covalent bond. For a complete synthesis protocol for PRN694, see Ref. 68.

The *in vitro* selectivity and potency of PRN694 against a panel of 250 kinases revealed a small number of inhibited kinase targets, of which only three non-TEC/non-Cys family kinases were inhibited >90% at 1 μM PRN694 (Fig. 1*D* and supplemental Table 1). Given the covalent nature of the binding of PRN694 to ITK and RLK, any kinase targets that do not contain a cysteine proximal to the kinase pocket that is susceptible to covalent binding are only temporarily inhibited due to drug clearance, yielding long term inhibition of only covalently bound kinases. To identify potential covalent targets of PRN694, we examined kinases that contain a cysteine homologous to Cys-442 in ITK using a microfluidic kinase assay. PRN694 exhibited high potency against ITK and RLK with IC_{50} values of 0.3 and 1.4 nM, respectively, as well as few off-target hits of significant potency (Fig. 1*E*). The IC_{50} for the family member TEC was also potent at 3.3 nM; however, we did not investigate further the kinetics of this interaction. In general, the biology of TEC in T-cells is less understood, but it does appear to serve a redundant role downstream of the T-cell receptor (33). The other TEC family member, BTK, had an IC_{50} of 17 nM; however, this interaction was reversible with only 27 ± 10 and 17 ± 12% occupancy of recombinant BTK after 6 and 24 h, respectively. Further kinetic analysis of PRN694 using the microfluidic kinase assay revealed time-dependent inhibi-

tion consistent with irreversible binding, providing k_{inact}/K_i values for both ITK (4.7 μM^{-1} s^{-1}) and RLK (0.46 μM^{-1} s^{-1}).

In vitro recombinant kinase-based selectivity assays do not always replicate the selectivity observed in cells due to the variable effects of higher cellular ATP concentrations and cellular pathway sensitivity to inhibition. Therefore, we tested PRN694 in the BioMap system (BioSeek, South San Francisco, CA) that screens inhibitory activities across a range of 12 primary human co-culture systems designed to replicate a variety of inflammatory conditions and disease states. This method has been previously utilized to study selectivity and cellular mechanism of action across a broad range of primary human cells (34–36). PRN694 demonstrated inhibitory activity only in cell systems in which T-cells were providing stimulatory readouts (Fig. 1*F*). No effects were observed in cell types that do not express ITK and RLK.

PRN694 Blocks TCR-induced Cellular and Molecular Activation—Given the strong *in vitro* potency and limited off-target activities, we wanted to confirm the T-cell-suppressive effects of PRN694. Because

A.

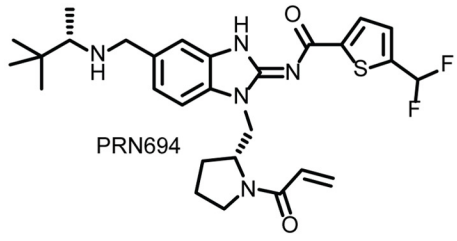

B.

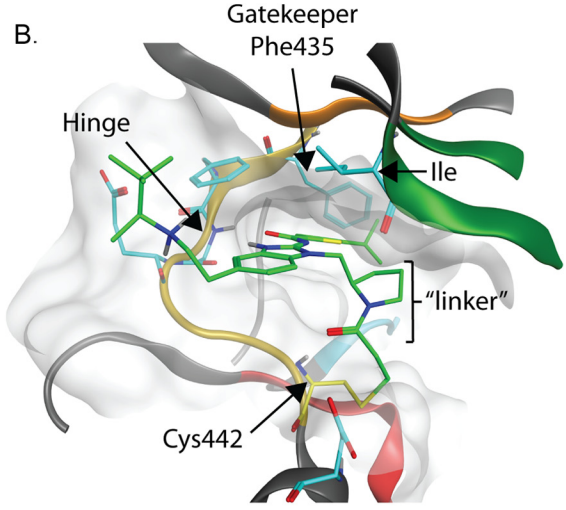

C.

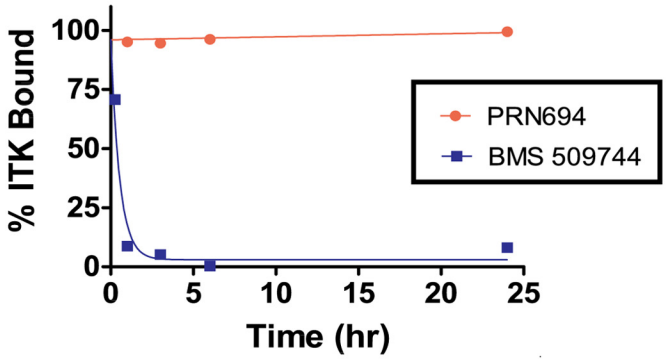

D.

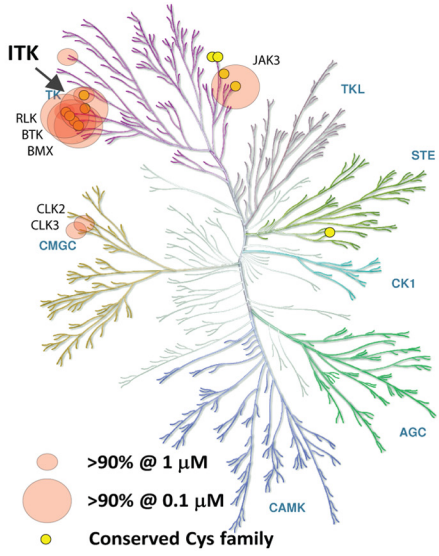

E.

Kinase	Biochemical IC_{50} (nM)
ITK	0.3
TEC	3.3
RLK	1.4
BTK	17
BLK	125
BMX	17
EGFR	2360
ERB-B2	>5000
ERB-B4	1820
JAK3	30

F.

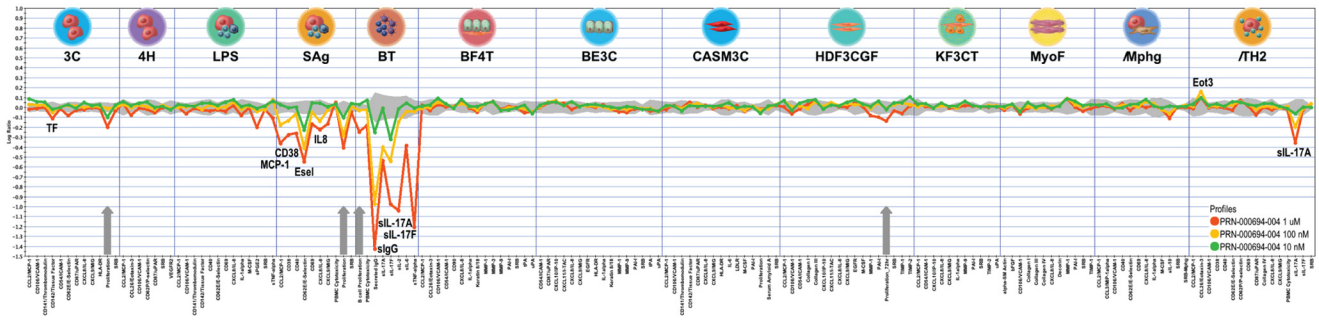

the molecular selectivity of PRN694 is achieved through Michael reaction chemistry, which covalently targets a cysteine moiety near the kinase active site, *in vivo* pharmacokinetics is mimicked *in vitro* by brief 30-min exposure followed by drug washout. To confirm that PRN694 inhibits TCR-induced activation, we examined membrane expression of CD69, a well established T-cell activation marker, 6 h after stimulation via anti-CD3 (Fig. 2*A*). With PRN694 pretreatment, CD3-mediated CD69 induction was inhibited both in Jurkat T-cells and freshly isolated primary CD4 or CD8 T-cells (Fig. 2, *B–D*). Maximal inhibition of CD69 induction was achieved with PRN694 concentrations ranging from 0.1 to 1.0 μM. For this study, we included tool compounds, including an inhibitor previously reported to inhibit ITK (BMS-509744), and the BTK-selective inhibitor PRN403 (also referred to as compound 8),[5] neither of which displayed T-cell inhibition (37). Note that BMS-509744 had relatively weak potency *in vitro*, consistent with the published data in cell-based assays (37). We chose the concentration of BMS-509744 to avoid the off-target effects we observed in BioMap screening of this compound (data not shown). As shown in Fig. 2, *E* and *F*, none of the tested compounds elicited T-cell cytotoxicity in these experiments.

The cellular CD69 activation analysis led us to investigate the effects PRN694 had on TCR-proximal molecular activation. We pretreated Jurkat cells with 0.5 μM PRN694 and then stimulated them with plate immobilized anti-CD3 and soluble anti-CD28 for 45 min. Immunoblot analysis of TCR activation pathways revealed that PRN694 blocked activation or nuclear translocation of NFAT1, JunB, pIκBα, and pERK (Fig. 2, *G* and *H*).

TCR-proximal Signaling and Calcium Flux Is Blocked by PRN694 in CD4 and CD8 T-Cells—CD4 helper and CD8 cytotoxic T-cells rely upon ITK and RLK to different extents (38); thus, we wanted to determine whether both T-cell subsets were susceptible to inhibition with PRN694. We purified CD4 or CD8 T-cells from healthy donor peripheral blood, pretreated each subset with 0.5 μM PRN694, and then stimulated with plate-immobilized anti-CD3 and soluble anti-CD28 for 45 min. Immunoblot analysis of proximal TCR activation pathways revealed that PRN694 blocks activation or nuclear translocation of NFAT1, JunB, pIκBα, and pPLCγ1-Y783 in both subsets (Fig. 3, *A–D*).

Robust and prolonged Ca^{2+} flux is a downstream component of TEC kinase signaling. To determine whether PRN694 inhibited Ca^{2+} flux, we pretreated Jurkat cells with various concentrations of PRN694 (from 1 nM to 1 μM) and loaded cells with the calcium flux indicator dye Fluo4AM. Calcium flux in response to anti-CD3 stimulation was then measured for 5 min. Results revealed inhibition of Ca^{2+} signaling with PRN694 at all concentrations above 1 nM as compared with the DMSO (vehicle) and BAPTA (negative control) treatments (Fig. 3, *E* and *F*). A modest dose response was observed that plateaued at concentrations greater than 25 nM.

To confirm that PRN694 blocks activation at a TCR-proximal site, we compared activation via CD3/CD28 with the PKC-activating phorbol 12-myristate 13-acetate combined with ionomycin, a calcium ionophore. As expected, PRN694 blocked NFAT, JunB, and IκBα activation only after CD3/CD28 stimulation, whereas phorbol 12-myristate 13-acetate/ionomycin stimulation circumvented this inhibitory activity (Fig. 3, *G* and *H*).

PRN694 Blocks FcR-induced Cellular and Molecular Activation in Primary NK Cells—ITK and RLK are critical components of NK cell FcR signaling. To study the effects of PRN694 in NK cells, we pretreated freshly isolated primary NK cells with 0.5 μM PRN694 for 30 min and then FcR-stimulated the cells for 45 min with plate-immobilized alemtuzumab (an anti-CD52 monoclonal antibody that potently activates FcR on NK cells). Immunoblot analysis revealed that PRN694 blocks alemtuzumab-induced activation or nuclear translocation of NFAT1, pIκBα, pERK, and pPLCγ1-Y783 (Fig. 4*A*).

CD107a and CD107b are two functional markers for NK cell activity. Their expression is up-regulated on NK cells upon FcR activation, indicating increased NK cell degranulation and cytotoxicity (39, 40). ITK has been shown to mediate FcR-initi-

[5] J. M. Bradshaw *et al.*, manuscript in preparation.

FIGURE 1. **Structure-based design and selectivity of the novel ITK/RLK inhibitor PRN694.** *A*, chemical structure of PRN694. *B*, model of PRN694 covalently bound to ITK. Molecular modeling predicts that the aminobenzimidazole scaffold makes two hydrogen bonds to the backbone amides of the hinge residues of the ATP binding pocket. The CF2-thiophene was found to provide high potency for either a phenylalanine or threonine gatekeeper residue. A methylpyrolidine linker presents the acrylamide in a position easily accessible for covalent bond formation with Cys-442. *C*, the dissociation of reversible *versus* irreversible inhibitors. Ligand binding to ITK as a function of time (hours) in a biochemical off-rate assay utilizing time-resolved FRET was determined as described under "Experimental Procedures." The completely reversible inhibitor BMS-509744 demonstrated extremely rapid dissociation from ITK (residence time (τ) = 32 $\pm$ 17 min), whereas PRN694 remained bound to ITK for the entire assay period, consistent with its irreversible covalent binding. *D*, the *in vitro* selectivity and potency of PRN694 against a panel of 250 kinases. Screening of PRN694 was performed at 0.1 and 1.0 μM. The results are displayed on a human kinase dendrogram (reproduced courtesy of Cell Signaling Technology, Inc.). *E*, PRN694 was tested in a microfluidics format kinase assay that separated phosphorylated from unphosphorylated peptide substrate based on capillary electrophoresis. PRN694 was tested against each target that contains a Cys in a homologous position to Cys-442 in ITK. IC_{50} values were calculated from plots of percentage inhibition of activity as a function of inhibitor concentration. All assays were performed at Nanosyn Inc. *F*, the BioMap cell screening panel (performed by BioSeek, South San Francisco, CA) is a set of cell-based assays used to understand the cellular potency and selectivity of inhibitory compounds. A variety of cell culture and co-culture systems are stimulated with a range of molecules. Biomarker readouts are measured as an indicator of various pathway activities in the culture systems. The biomarker readouts measured in each system are indicated along the *x* axis. The *y* axis shows the log10 expression ratios of the readout level measurements relative to solvent (DMSO buffer) controls. Three concentrations of PRN694 were tested for the ability to modulate the various readouts. The three culture systems that showed dose-dependent modulation of biomarkers in response to PRN694 were the SAg system, the BT system, and the TH2 system. The SAg system consists of primary human umbilical vein endothelial cells cultured with peripheral blood mononuclear cells stimulated with superantigens. The BT system consists of B cells co-cultured with peripheral blood mononuclear cells stimulated with anti-IgM and mild T-cell receptor stimulation. The TH2 system consists of primary human umbilical vein endothelial cells co-cultured with 14-day TH2 polarized CD4 T-cell blasts stimulated with TCR and IL-2. PRN694 had essentially no inhibitory activity in cell types that do not express ITK and RLK, including 3C (venular endothelial cells (HuVEC)/IL-1β, TNF, and IFNγ), 4H (HuVEC/IL-4 and histamine), LPS (PBMC and HuVEC/LPS), BF4T (bronchial epithelial cells and human dermal fibroblasts/TNF and IL-4), BE3C (bronchial epithelial cells/IL-1β, TNF, and IFNγ), CASM3C (coronary artery smooth muscle cells/IL-1β, TNF, and IFNγ), HDF3CGF (human dermal fibroblasts/IL-1β, TNF, IFNγ, epidermal growth factor, basic fibroblast growth factor, and platelet-derived growth factor-BB), KF3CT (keratinocytes and dermal fibroblasts/IL-1β, TNF, and IFNγ), MyoF (lung fibroblasts/TNF and TGF-β), and Mphg (HuVEC and macrophages/TLR2). Weak inhibitory signals were only detected at the highest PRN694 concentration in the venular endothelia system (3C), the PBMC/HUVEC system (LPS), and the human dermal fibroblast system (HDF3CGF), potentially due to low level off-target effects.

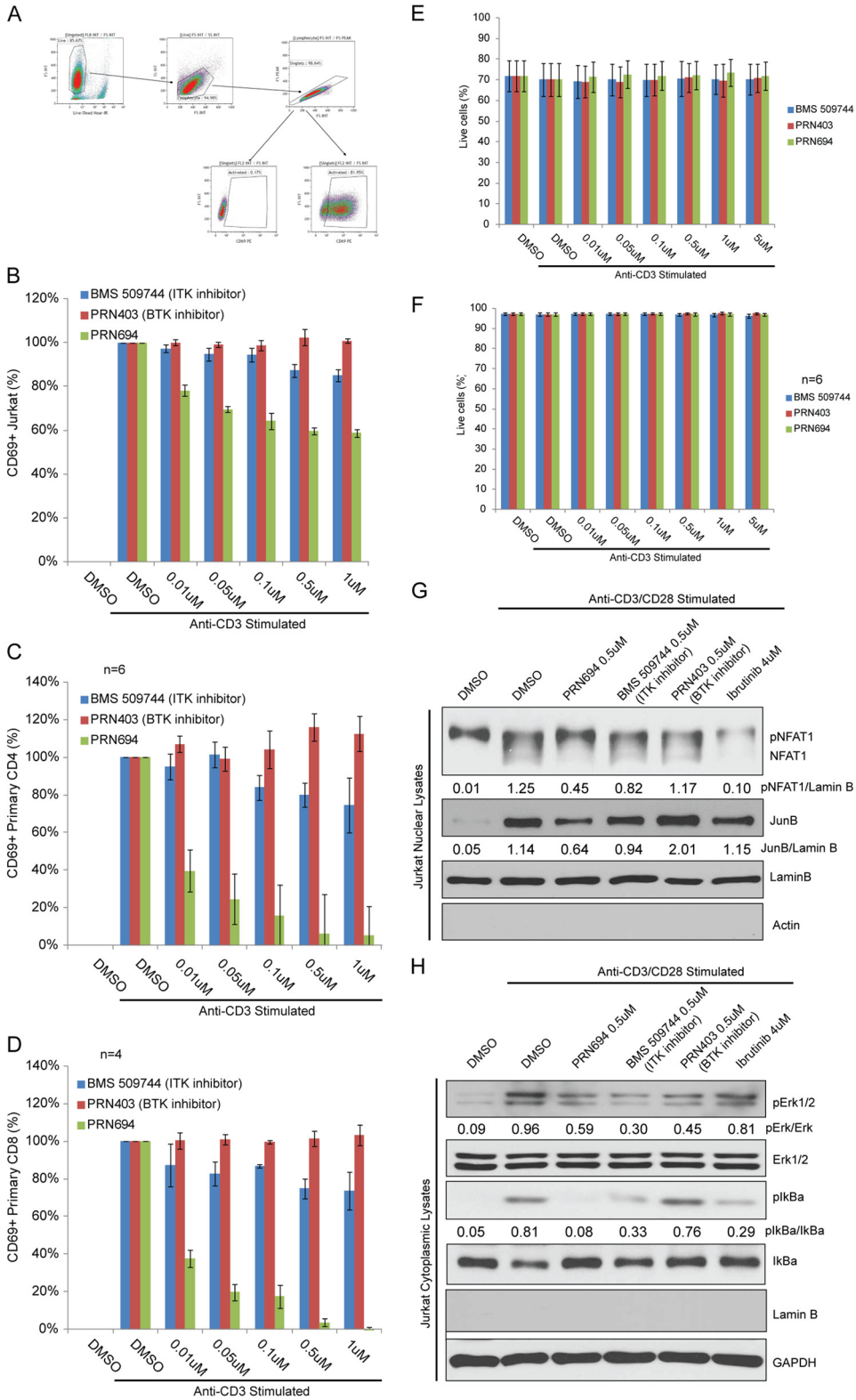

FIGURE 2. **PRN694 blocks cellular and molecular activation of T-lymphocytes and the Jurkat T-ALL cell line.** *A*, gating strategy for flow cytometric analysis of CD69 surface expression in Jurkat cells. Singlet live lymphocytes were gated for CD69 surface expression in Jurkat cells. Jurkat cells ($n = 4$) (*B*), human primary CD4 T-cells ($n = 6$) (*C*), or human primary CD8 T-cells ($n = 4$) (*D*) were pretreated for 30 min with PRN694, BMS-509744, or PRN403 at the indicated doses or vehicle (DMSO), subjected to stimulation with anti-CD3/anti-CD28 for 6 h, and analyzed via flow cytometry for CD69 surface expression. Baseline (unstimulated) CD69 percentage was subtracted, and data were normalized to stimulated and vehicle-treated sample. Jurkat cells (*E*) or CD3 T-cells (*F*) isolated from healthy donors were pretreated with vehicle (DMSO), PRN694, BMS-509744, or PRN403 at the indicated doses and stimulated with anti-CD3/anti-CD28 for 6 h. Cell viability was evaluated by flow cytometry using LIVE/DEAD® stain (Invitrogen). Nuclear (*G*) or cytoplasmic (*H*) extracts from Jurkat cells pretreated for 30 min with 0.5 μM PRN694, 0.5 μM BMS-509744, 0.5 μM PRN403, 4 μM ibrutinib, or vehicle (DMSO) and stimulated with anti-CD3/anti-CD28 for 45 min were analyzed by immunoblot. Antibodies to actin, lamin B, and GAPDH were included as controls for nuclear *versus* cytoplasmic extractions. Data are representative of three experiments. For immunoblots *G* and *H*, densitometric ratios between phosphoprotein and total or loading control are provided. *Error bars*, S.E.

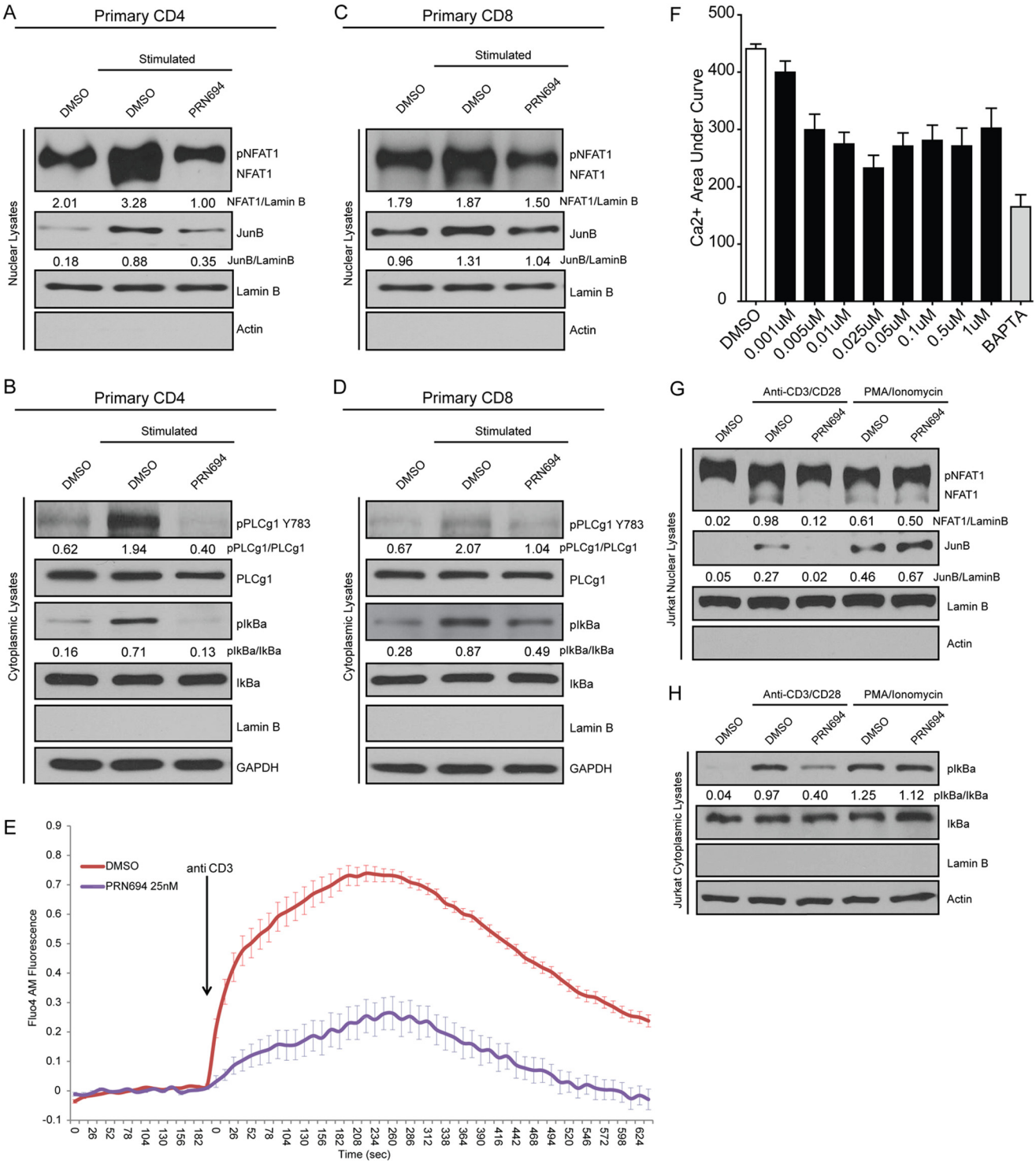

FIGURE 3. **TCR-proximal signaling is irreversibly blocked by PRN694, abrogating downstream pathway activation.** *A* and *B*, freshly isolated primary CD4 T-cells were preincubated with vehicle (DMSO) or PRN694 (0.5 μM) and then stimulated for 45 min with anti-CD3/anti-CD28 antibodies. Nuclear extracts (*A*) or cytoplasmic extracts (*B*) were analyzed by immunoblot with the indicated antibodies. *C* and *D*, freshly isolated primary CD8 T-cells were treated as described for CD4 cells, and nuclear (*C*) and cytoplasmic (*D*) extracts were analyzed by immunoblot. *E*, Jurkat cells were pretreated with 25 nM PRN694 or vehicle, labeled with Fluo4AM, and then stimulated by the addition of anti-CD3 indicated by an *arrow*. Calcium flux was measured using the intensity of Fluo-AM measured over 5 min following the addition of anti-CD3. The graph shows cumulative data from 12 replicates conducted over two separate experiments. *F*, Jurkat cells were pretreated with PRN694 (1 nM to 1 μM), vehicle (DMSO), or BAPTA-AM (13 μM); labeled with Fluo4AM; and then stimulated by the addition of anti-CD3. Calcium flux was measured using the intensity of Fluo-AM measured over 5 min following the addition of anti-CD3. The graph shows the area under the fluorescent intensity/time curve. *G* and *H*, Jurkat cells were pretreated with 0.5 μM PRN694 or vehicle (DMSO) and then stimulated either with anti-CD3/anti-CD28 or 50 ng/ml phorbol 12-myristate 13-acetate plus 1 μg/ml ionomycin for 45 min. Nuclear (*G*) and cytoplasmic (*H*) extracts were analyzed by immunoblot. For immunoblots A, B, C, D, G, and H, densitometric ratios between phosphoprotein and total or loading control are provided. *Error bars*, S.E.

ated cytotoxicity (2). To determine whether PRN694 inhibits FcR-induced activation of NK cells, we examined membrane expression of CD107a/b in primary NK cells stimulated with plate-coated alemtuzumab for 6 h. FcR-induced CD107a/b expression was significantly inhibited by PRN694 in a dose-dependent manner ($p < 0.05$) (Fig. 4*B*).

A primary functional readout of NK cell FcR activation is the ability to lyse antibody-coated cells in an antibody-dependent cellular cytotoxicity assay. To examine the impact of PRN694 on this functional readout, we pretreated primary human NK cells with varying concentrations of PRN694 or the BTK inhibitor PRN403 and used these cells at a 25:1 effector/target ratio with humanized anti-CD20 rituximab biosimilar-coated Jeko-1 targets. The data showed that PRN694 significantly attenuated NK cell FcR-induced killing at concentrations exceeding 0.37 μM, whereas PRN403 did not alter killing, and isotype-coated Jeko-1 cells induced negligible killing as expected (Fig. 4*C*).

Given that macrophages, dendritic cells, and mast cells also express and utilize Fc receptors, we sought to examine the effects of PRN694 on these unique cell types. Primary human monocyte-derived macrophages and dendritic cells were pretreated with 0.5 μM PRN694 and FcR-stimulated using immobilized human IgG. Cytokine production shows that PRN694 had no impact on either cell type because macrophage production of TNF and dendritic cell production of IL-12 and TNF was unaffected by PRN694 (Fig. 5, *A–C*). In addition, the Fcϵ-expressing mast cell line RBL-2H3 was stimulated by coating the cells with anti-DNP IgE and subsequently exposing the cells to DNP. Histamine release after exposure to 0.5 μM PRN694 was unaffected (Fig. 5*D*). Furthermore, molecular activation of ERK1/2 following stimulation was unaltered (Fig. 5*E*). ITK expression was not detectable in the dendritic cells, macrophages (data not shown), or RBL-2H3 mast cells we used (41). Overall, these results indicate that in NK cells, but not in dendritic, macrophage, or RBL-2H3 mast cells, which do not express ITK and RLK, FcR-induced stimulation is curtailed by PRN694.

PRN694 Selectively Inhibits ITK and RLK Kinase Activity—Collectively, our data show that PRN694 binds irreversibly to the non-kinase-essential cysteine 442 located in the hinge region of ITK. Therefore, a cysteine to alanine mutation at this site is predicted to yield an active, drug-resistant version of ITK (ITK-C442A). Because Jurkat cells do not express RLK, they rely solely upon ITK for propagation of the TCR signal; therefore, expression of ITK-C442A should render these cells resistant to PRN694 (28). In anti-CD3/CD28-activated Jurkat cells expressing ITK-WT, 0.5 μM PRN694 inhibited the downstream TCR signaling, including nuclear activation of NFAT1 and cytoplasmic PLCγ1 and IκBα, as expected (Fig. 6*A*). However, PRN694 was not able to inhibit these same downstream TCR pathways in Jurkat cells that stably express ITK-C442A (Fig. 6*B*). Total ITK protein expression was comparable among parental Jurkat, Jurkat ITK-WT, and Jurkat ITK-C442A cell lines with or without stimulation (Fig. 6*C*). Notably, the C442A mutant did not completely rescue inhibition by PRN694, potentially because the C442A cells also express endogenous ITK-WT, which would be susceptible to inhibition, or because of low level inhibition of additional kinases at 0.5 μM PRN694. These data confirm that ITK is a primary molecular target of PRN694 and that the Cys-442 moiety is critical for the capacity of PRN694 to inhibit ITK. Ibrutinib, which inhibits both BTK and ITK in a Cys-dependent manner, also lost potency in the ITK-C442A-expressing cells, as we have previously shown (28). As expected, the BTK-selective compound PRN403 had no inhibitory activity in either cell line, supporting the hypothesis that the ITK-inhibiting activity of PRN694 was driving its effect. The non-covalent BMS-509744 displayed only weak inhibitory activity.

In certain subsets of T-cells and NK cells, RLK can compensate for inhibition or loss of ITK (42). Therefore, an ITK/RLK combined inhibitor can potentially more effectively block systemic TCR-induced activation. Immunoblot analysis revealed that both PRN694 and the BTK/ITK inhibitor ibrutinib could block downstream TCR signaling via PLCγ1, IκBα, and NFAT1 in anti-CD3/CD28-stimulated, empty vector-transduced, control Jurkat cells (Fig. 6*D*). BMS-509744 was weakly active against TCR-stimulated signals. Critically, however, only the combined ITK/RLK inhibitor PRN694 was able to ablate TCR-induced molecular activation in Jurkat cells that stably express RLK (Fig. 6*E*). These data confirm that PRN694 is a dual inhibitor of ITK and RLK and can block downstream TCR activation in cells that express both complementary TEC kinases.

PRN694 Inhibits TCR-induced Primary T-cell Proliferation without Direct Cytotoxicity—Rapid and robust cellular proliferation is a hallmark functional readout of TCR stimulation. To characterize the effect of PRN694 on TCR-induced proliferation, CD3 T-cells isolated from healthy donors were stained with 1 μM CFSE, pretreated with 0.1 μM PRN694 or control inhibitor BMS-509744, PRN403, or ibrutinib for 30 min, and then stimulated with anti-CD3/CD28 for 6 days. Day 6 flow cytometry analysis revealed that PRN694 significantly inhibited the anti-CD3/CD28-induced proliferation of both CD4 and CD8 T-cells ($p < 0.01$) (Fig. 7*A*). This attenuation of TCR-induced cellular division index was not achieved by BMS-509744, the BTK/ITK inhibitor ibrutinib, or the BTK inhibitor PRN403 (Fig. 7, *B* and *C*).

Conceivably, a cytotoxic inhibitor could halt TCR-induced proliferation in a non-selective manner. Therefore, we investigated apoptosis and cell death by annexin V/propidium iodide flow cytometry analysis. These data demonstrate that PRN694 is not directly cytotoxic to healthy CD3 T-cells (Fig. 7*D*), supporting the notion that PRN694 prevents TCR-induced proliferation by blocking specific kinases necessary to initiate molecular signals that drive cellular activation and subsequent proliferation.

PRN694 Inhibits Proinflammatory Cytokine Release by Primary T-cells and Functional T-cell Cytotoxicity—ITK and RLK are critically important for the production of proinflammatory cytokines and inflammatory disease (43). We sought to examine the effect of PRN694 on proinflammatory cytokine production. Freshly isolated CD3 T-cells from healthy donors were pretreated with vehicle (DMSO) or 0.1 μM PRN694, BMS-509744, or PRN403 for 30 min and then stimulated with anti-CD3/CD28 for 48 h. Soluble cytokines were assayed by a cyto-

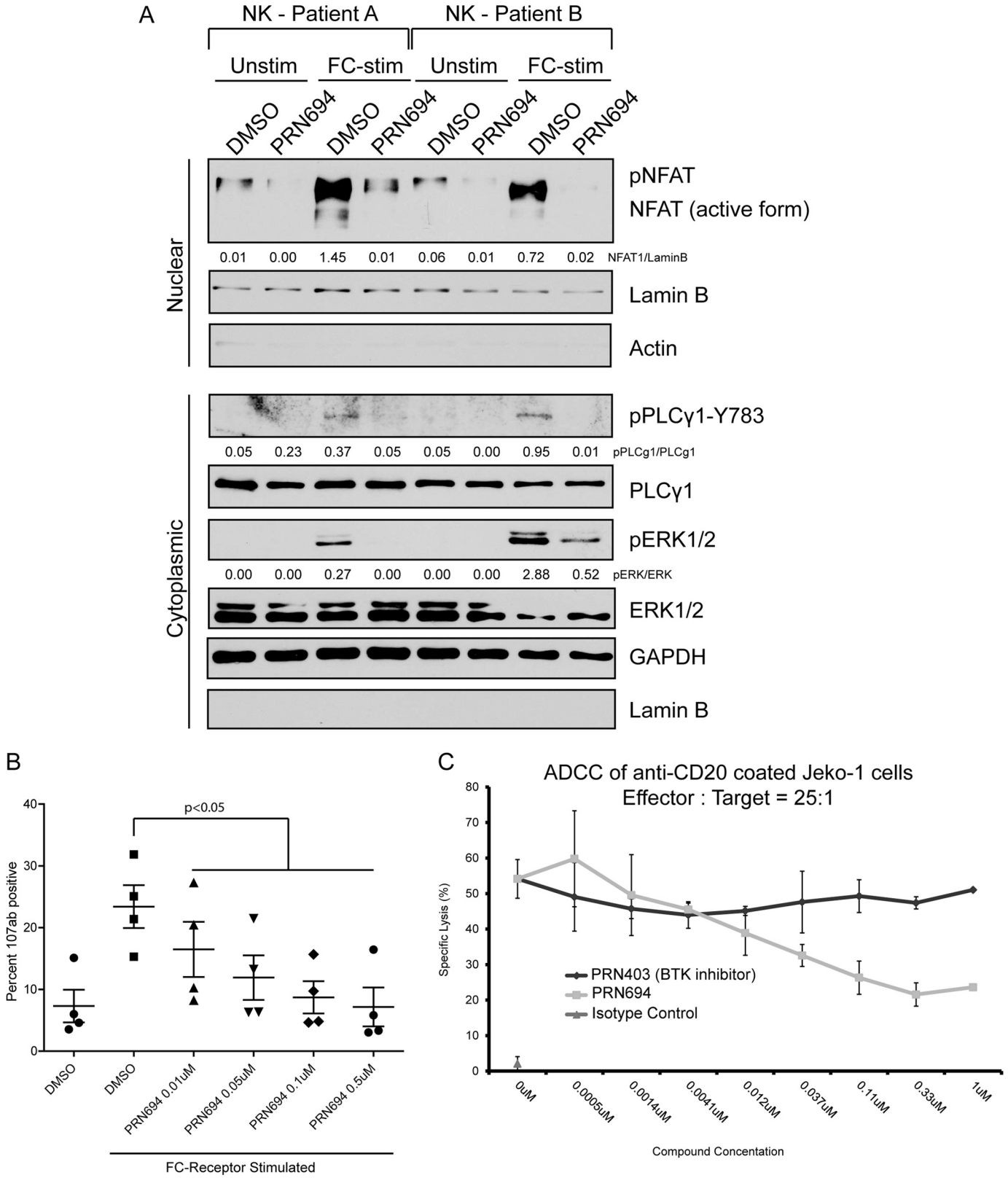

FIGURE 4. **PRN694 blocks Fc receptor-induced cellular and molecular activation in primary NK cells.** *A*, immunoblot analysis of nuclear and cytoplasmic extracts from freshly isolated healthy primary NK cells pretreated with 0.5 μM PRN694 or vehicle (DMSO) and stimulated with plate-coated alemtuzumab (10 μg/ml) for 45 min. *B*, healthy primary NK cells were pretreated with PRN694 at several doses or with vehicle (DMSO) and then stimulated with plate-coated alemtuzumab (10 μg/ml) for 6 h. Surface expression of CD107a/b was analyzed via flow cytometry. Data show the percentage of positive cells of the purified NK cell population. *C*, health primary NK effector cells were isolated from PBMCs and pretreated with PRN694 or PRN403 at the indicated concentrations. Effector cells were cultured at a 25:1 ratio with 1 μg/ml rituximab biosimilar-coated Jeko-1 target cells for 16 h. Specific lysis of target cells was quantified by measuring lactate dehydrogenase release into the supernatant. Isotype-coated target cells were used as a non-killing control. *Error bars*, S.E. For all immunoblots, densitometric ratios between phosphoprotein and total or loading control are provided.

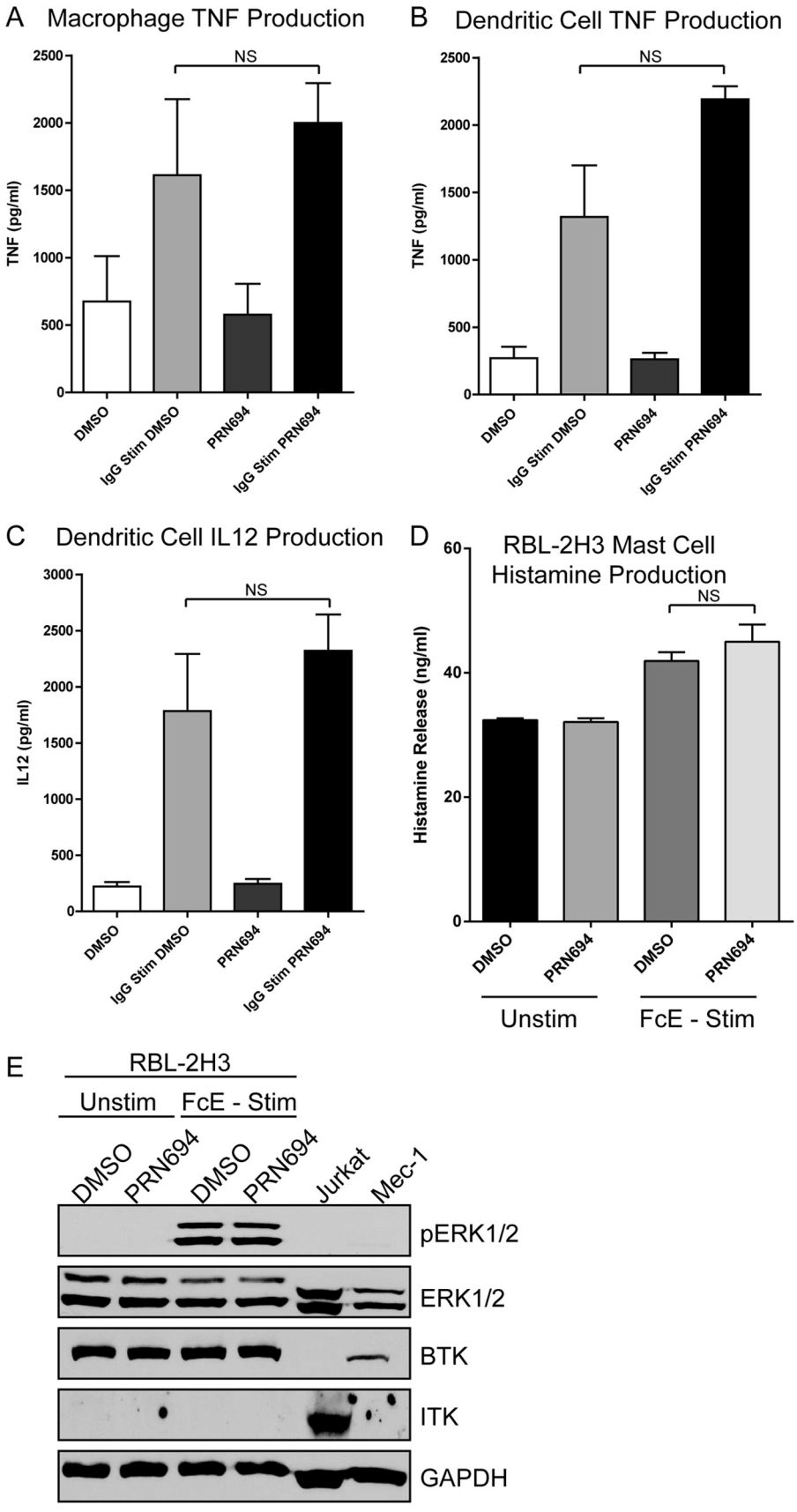
A
Macrophage TNF Production
TNF (pg/ml)
2500
2000
1500
1000
500
0
NS
DMSO
IgG Stim DMSO
PRN694
IgG Stim PRN694
B
Dendritic Cell TNF Production
TNF (pg/ml)
2500
2000
1500
1000
500
0
NS
DMSO
IgG Stim DMSO
PRN694
IgG Stim PRN694
C
Dendritic Cell IL12 Production
IL12 (pg/ml)
3000
2500
2000
1500
1000
500
0
NS
DMSO
IgG Stim DMSO
PRN694
IgG Stim PRN694
D
RBL-2H3 Mast Cell
Histamine Production
Histamine Release (ng/ml)
60
40
20
0
NS
DMSO
PRN694
DMSO
PRN694
Unstim
FcE - Stim
E
RBL-2H3
Unstim
FcE - Stim
DMSO
PRN694
DMSO
PRN694
Jurkat
Mec-1
pERK1/2
ERK1/2
BTK
ITK
GAPDH

metric bead assay, revealing that IL-2, TNFα, and IFNγ levels were significantly lower in cultures from PRN694-treated cells (Fig. 7, *E–G*). Neither BMS-509744 nor the control BTK inhibitor PRN403 altered cytokine levels.

$CD4^+$ Th17 cells are critical proinflammatory components of the adaptive immune system implicated in multiple autoimmune diseases, such as psoriasis, multiple sclerosis, and inflammatory bowel disease (44). To investigate the suppression of Th17 cells by PRN694, we pre-enriched healthy donor PBMCs for $CD4^+/CXCR3^-/CCR6^+$ cells, which include a high fraction of Th17 cells. This enriched fraction was then pretreated with vehicle or 0.5 μM PRN694, BMS-509744, or PRN403 and stimulated with anti-CD3/anti-CD28 for 12 h. PRN694 significantly inhibited TCR-induced Th17 cell activation as measured by intracellular levels of IL-17a (Fig. 7*H*).

To examine the functional effects of PRN694 on mature primary human CD8 T-cells, we conducted allogeneic mixed lymphocyte reactions using ^{51}Cr-loaded PBMCs as targets at a 50:1 effector/target ratio (Fig. 7*I*). Our results show that 0.5 μM PRN694 pretreatment significantly attenuates CD8 T-cell cytotoxicity after allogeneic stimulation ($p = 0.0099$).

PRN694 Attenuates TCR-induced Activation of T-cell Prolymphocytic Leukemia (T-PLL)—To explore a potential therapeutic application of PRN694 in T-cell leukemia, we examined the mRNA expression of ITK in primary T-cell leukemia cells to confirm relevant levels of target expression. Leukemic T-cells from T-PLL patients ($n = 13$) expressed mRNA levels of ITK that were indistinguishable from healthy T-cells ($n = 4$) (Fig. 8*A*). Using the HH cutaneous T-cell lymphoma cell line, we found that PRN694 effectively blocked anti-CD3/anti-CD28-induced TCR stimulation of NFAT1, JunB, PLCγ1, and IκBα (Fig. 8*B*). Next, we analyzed the effects of PRN694 on anti-CD3/anti-CD28-induced phosphorylation of PLCγ1 in T-PLL patient cells as detected by phosphoflow cytometry (Fig. 8*C*) and immunoblotting (Fig. 8*D*). As expected for ITK/RLK inhibition, phosphorylation of the upstream molecule ZAP70 was not blocked. Because TCR-driven signaling events are important in the survival and growth of T-cell tumors, these *ex vivo* data suggest a potential clinical application of this compound in the treatment of T-cell leukemias.

In Vivo Inhibition of a Delayed Type Hypersensitivity Reaction in Mice by PRN694—Having demonstrated the kinase selectivity and *in vitro*/*ex vivo* potency of PRN694, the next important step was to examine its pharmacokinetic and pharmacodynamic profile in mice. Following a single 20 mg/kg intraperitoneal dose of PRN694, thymocytes were harvested from mice at the time points of 1, 6, and 14 h in order to measure the binding of PRN694 to ITK in T-cells. To measure the target occupancy by PRN694, thymocytes were treated with a fluorescently labeled probe that binds specifically and irreversibly to unoccupied ITK. The PRN694 occupancy of ITK was 98, 95, and 54% at 1, 6, and 14 h, respectively (Fig. 9*A*). Plasma was also harvested at those three time points following administration of PRN694. As determined by mass spectrometry, the concentrations of PRN694 in the plasma were 2.8, 0.66, and 0.027 μM at 1, 6, and 14 h, respectively (Fig. 9*A*). At 14 h, the plasma level of PRN694 was over 10-fold lower than the IC_{50} in whole blood as measured by TCR-stimulated IL-2 production (data not shown). Therefore, the occupancy of ITK at 14 h (54%) was due to a durable pharmacodynamic effect rather than continued exposure by circulating PRN694. This is consistent with the extended *in vitro* occupancy demonstrated in Fig. 1*C*. Note that although the binding of PRN694 to ITK is irreversible, the drop in occupancy over time *in vivo* is expected due to turnover of the target in cells.

ITK and RLK play critical roles in T-cell-driven inflammation (43). Therefore, we tested the effect of PRN694 in an oxazolone-induced DTH reaction, a well established *in vivo* model of inflammation driven by cell-mediated immunity. In this hapten-driven type IV hypersensitivity reaction, the cell-mediated response is predominantly driven by Th1 cells (45). Mice were sensitized with oxazolone on the shaved abdomen and then challenged with oxazolone or vehicle 7 days later on both sides of the right or left ear, respectively. One hour prior to the challenge, mice were dosed via intraperitoneal injection with vehicle control, 0.5 mg/kg dexamethasone (positive control), or PRN694 at 20 mg/kg. Twenty-four hours after the challenge, ear edema was measured by weighing 7-mm ear cores. PRN694 treatment resulted in significantly lower weights relative to vehicle ($p < 0.05$), indicating inhibition of the DTH reaction (Fig. 9*B*). This result demonstrates the ability of PRN694 to impact Th1 cell activity *in vivo* (38).

DISCUSSION

Many human diseases and conditions are mediated or exacerbated by aberrant activation of T-cells or NK cells. Because T-cell activation invariably relies on TCR-mediated signaling and NK cells are activated via the FcR, agents that can selectively interrupt these pathways would be of significant clinical benefit. Given that ITK and RLK are key components of both TCR and FcR signaling, a compound with selectivity for these two targets should provide a useful chemical biology tool to impact these important cell populations. Here, we describe the discovery, biochemical characterization, and biological assessment of PRN694, a novel lead that selectively and irreversibly inhibits both of these critical lymphocyte kinases. We demonstrate that PRN694 has the desired potency and selectivity for ITK and RLK, as shown by *in vitro* kinase assays and experiments in Jurkat T-cells with mutated ITK or overexpressed RLK. We further show that TCR or FcR-induced cellular and molecular activation, TCR-induced T-cell proliferation, and proinflammatory cytokine release are inhibited by PRN694. Moreover, we demonstrate extended *in vivo* pharmacodynamic

FIGURE 5. **PRN694 does not inhibit FcR-induced macrophage, dendritic cell, or mast cell activation.** Monocyte-derived macrophages (*A*) or dendritic cells (*B*) were stimulated with immobilized human IgG for 24 h. Supernatant levels of TNF were measured. *C*, monocyte-derived dendritic cells were stimulated with immobilized human IgG for 24 h. Supernatant levels of IL-12 were measured. *A–C*, data are derived from three individual experimental donors. *E*, RBL-2H3 mast cells were coated with anti-DNP IgE and subsequently stimulated with DNP for 30 min. Supernatant levels of histamine were measured via ELISA. *F*, RBL-2H3 mast cells were coated with anti-DNP IgE and subsequently stimulated with DNP for 30 min. Molecular activation was characterized by immunoblot analysis of pERK1/2. In addition, BTK and ITK expression were tested. Jurkat and Mec-1 cells were included as ITK- and BTK-expressing controls. *NS*, not significant. *Error bars*, S.E.

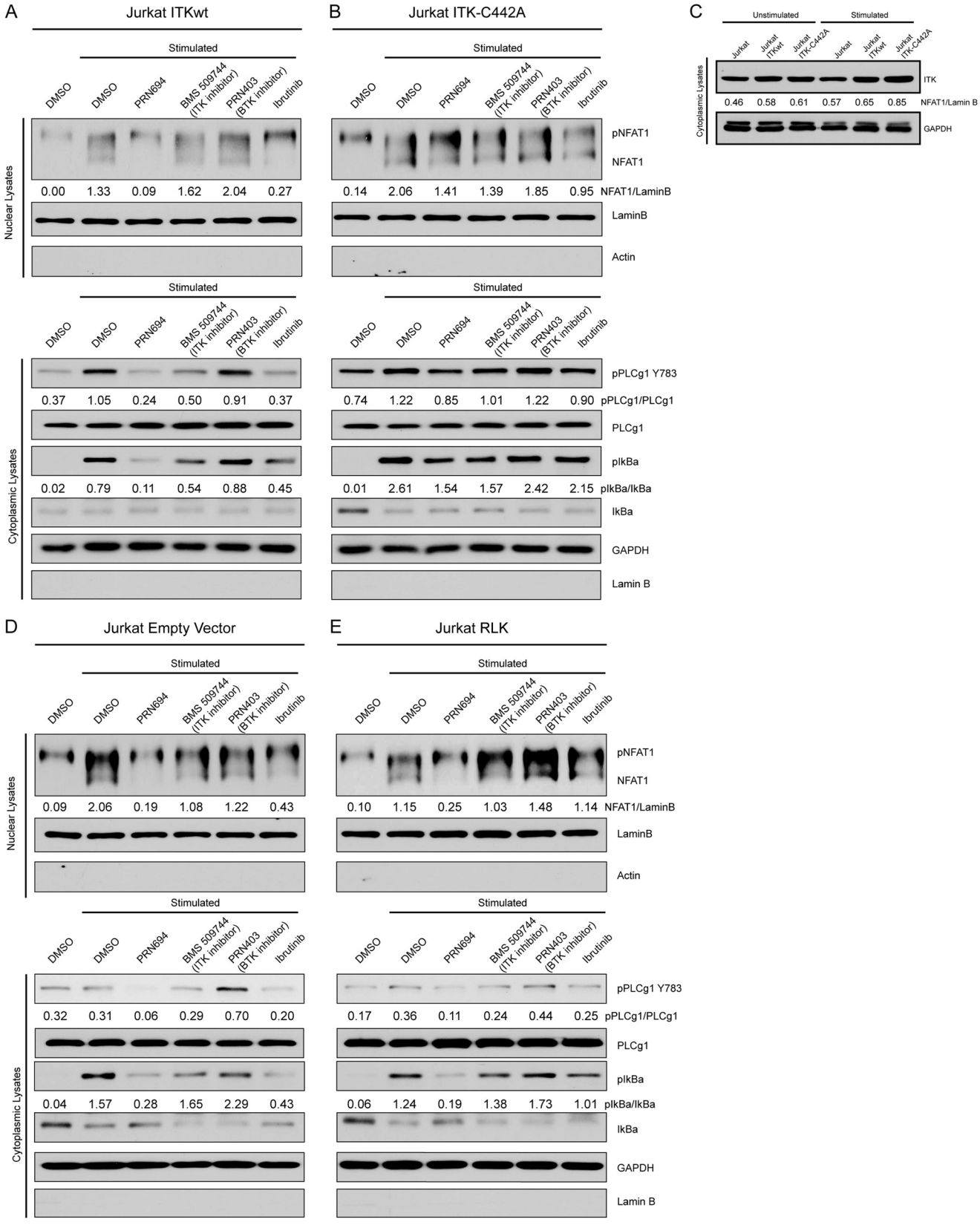

FIGURE 6. **PRN694 selectively inhibits ITK and RLK kinase activity.** Shown is immunoblot analysis of Jurkat ITK-WT (*A*) and Jurkat ITK-C442A (*B*) nuclear and cytoplasmic lysates after pretreatment with 0.5 μM PRN694, 0.5 μM BMS-509744, 0.5 μM PRN403, 1 μM ibrutinib, or vehicle (DMSO) followed by stimulation with anti-CD3/anti-CD28 for 45 min. *C*, immunoblot analysis of cytoplasmic lysates from parental Jurkat, Jurkat ITK-WT, and Jurkat ITK-C442A cell lines with or without anti-CD3/CD28 stimulation for 45 min. Blots were probed with ITK and GAPDH. Immunoblot analysis of Jurkat-EV (empty vector) (*D*) and Jurkat-RLK (*E*) nuclear and cytoplasmic lysates after pretreatment with 0.5 μM PRN694, 0.5 μM BMS-509744, 0.5 μM PRN403, 1 μM ibrutinib, or vehicle (DMSO) followed by stimulation with anti-CD3/anti-CD28 for 45 min. For all immunoblots, densitometric ratios between phosphoprotein and total or loading control are provided.

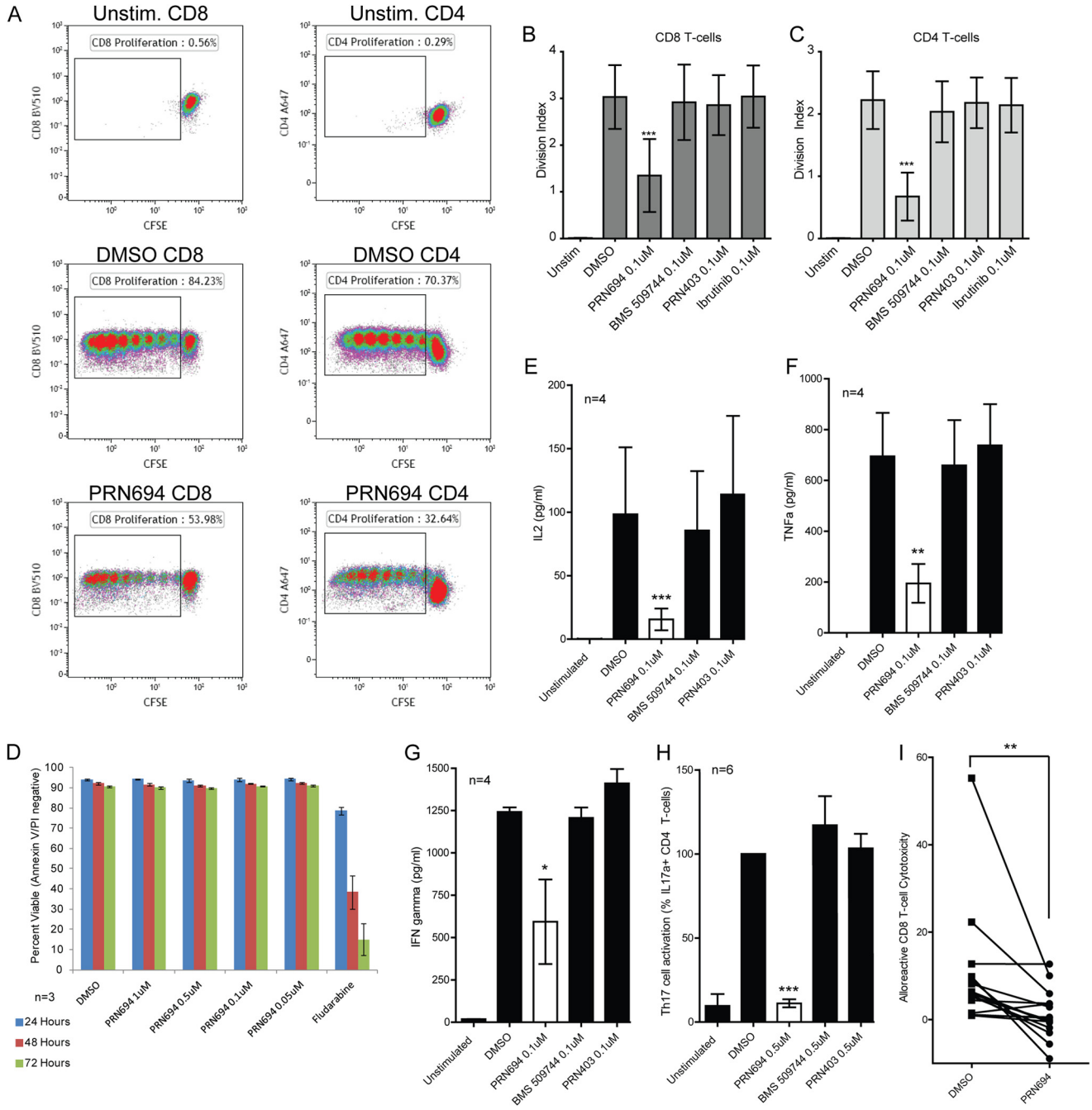

FIGURE 7. **PRN694 inhibits TCR-induced primary T-cell proliferation and proinflammatory cytokine production without direct cytotoxicity.** CD3 T-cells isolated from healthy donors ($n = 3$) were stained with 1 μM CFSE; pretreated with 0.1 μM PRN694, 0.1 μM PRN869, 0.1 μM PRN403, or 0.1 μM ibrutinib for 30 min; and then incubated without or with anti-CD3/CD28 for 6 days. *A*, representative flow cytometry analysis of CFSE staining. Shown is a graphical representation of results for CD8 T-cells (*B*) and CD4 T-cells (*C*). The division index is the average number of cell divisions that a cell in the original population has undergone. *D*, cytotoxicity of PRN694 in primary healthy T-cells. CD3 T-cells were isolated from healthy donors ($n = 3$), pretreated with PRN694 as indicated, and analyzed by annexin/propidium iodide flow cytometry at 24, 48, and 72 h. Data show absolute percentages of CD3-positive cells negative for both annexin and propidium iodide. *E–G*, CD3 T-cells from healthy donors ($n = 4$) were pretreated with or without 0.1 μM PRN694, 0.1 μM BMS-509744, 0.1 μM PRN403, or vehicle (DMSO) for 30 min and then stimulated with anti-CD3/CD28 for 48 h. Cytokines, including IL-2 (*E*), TNF (*F*), and IFNγ (*G*), present in the supernatant were assayed by a cytometric bead assay. *H*, effect of PRN694 on TCR-induced Th17 activation. PBMCs from healthy donors ($n = 6$) were pre-enriched for $CD4^+/CXCR3^-/CCR6^+$ cells, which include a high fraction of Th17 cells. These cells were pretreated with vehicle (DMSO), 0.5 μM PRN694, 0.5 μM BMS-509744, or 0.5 μM PRN403 and then stimulated with anti-CD3/anti-CD28 for 12 h. TCR-induced intracellular IL-17a was detected by flow cytometry. Data are shown as the percentage of IL-17a-positive CD4 T-cells normalized to DMSO. *I*, healthy primary CD8 T-cells were pretreated with 1 μM PRN694 or DMSO control and subsequently cultured at a 25:1 ratio with ^{51}Cr-labeled allogeneic PBMCs for 4 h. Afterward, specific lysis of allogeneic PBMCs was quantified by measurement of released ^{51}Cr as compared with maximum and minimum lysis controls. For all figures: *, $p < 0.05$, **, $p < 0.01$, ***, $p < 0.001$. *Error bars*, S.E.

effects and efficacy in inhibiting DTH in a well characterized murine model system.

Consistent with our CD4 and CD8 T-cell data using PRN694, studies from ITK- and RLK-deficient mice demonstrate the critical roles these two TEC kinases play in T-cell and NK cell signaling (3). ITK-deficient mice display defects in TCR-induced T-cell responses, including proliferation, cytokine production, and activation of downstream pathways (46, 47), and

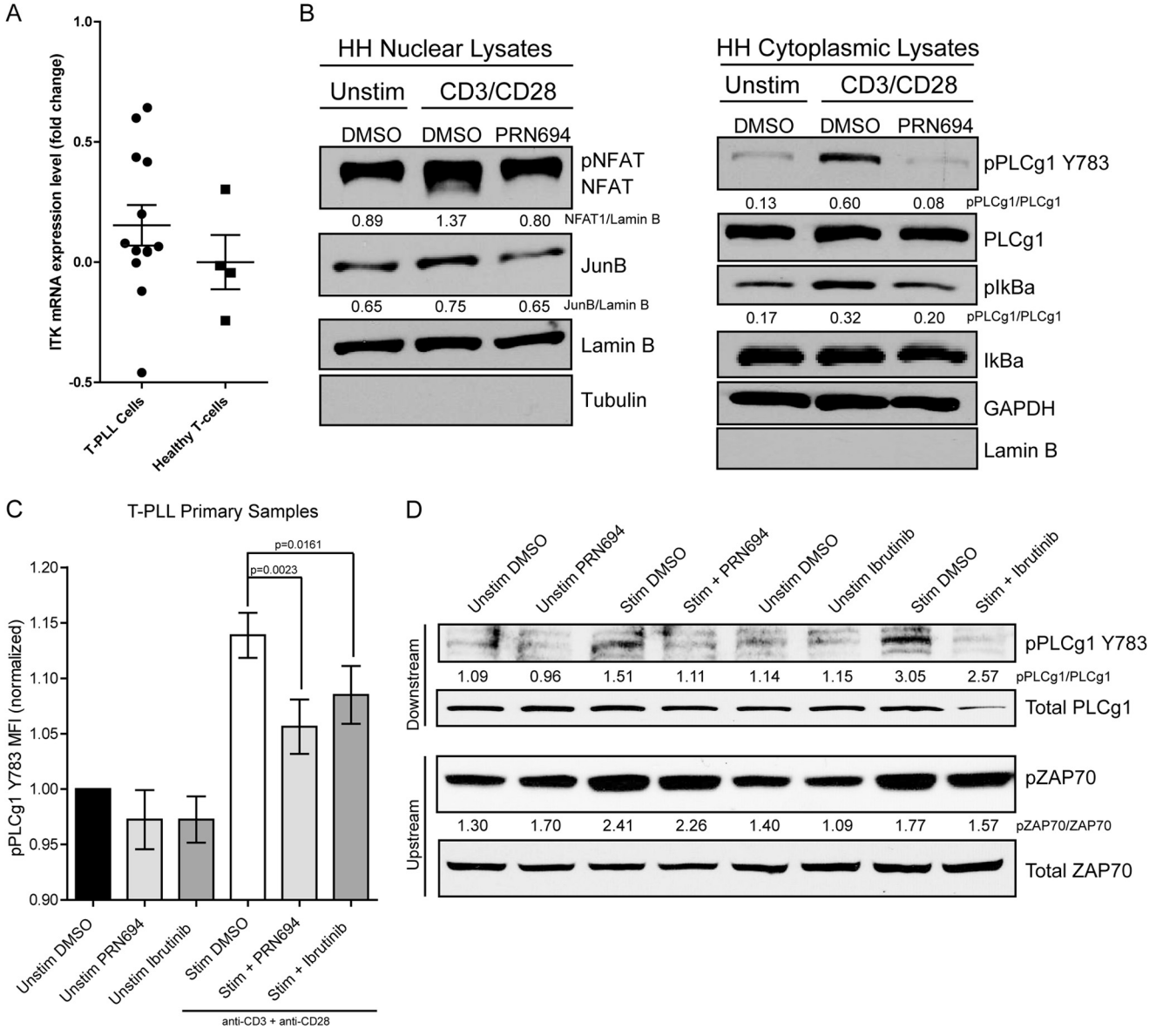

FIGURE 8. **PRN694 attenuates TCR-induced signaling in primary human T-PLL.** *A*, total RNA from 13 cryopreserved primary T-PLL samples and 4 healthy donors was interrogated for ITK and GAPDH mRNA by quantitative RT-PCR. -Fold change relative to GAPDH is represented along with the mean and S.E. *B*, HH cells were pretreated with DMSO or 0.1 μM PRN694 for 30 min and then stimulated with anti-CD3/anti-CD28 for 45 min. Nuclear and cytoplasmic cellular extracts were interrogated for activation of NFAT1, JunB, PLCγ1-Y783, and IκBα. *C*, primary cryopreserved T-PLL samples ($n = 8$) were stimulated via anti-CD3/anti-CD28 for 45 min, and pPLCγ1-Y783 was examined by phosphoflow cytometry. The mean fluorescence intensity for each sample was normalized to unstimulated. *D*, immunoblot analysis of TCR-induced (anti-CD3/anti-CD28 for 45 min) primary T-PLL cells freshly obtained from peripheral blood. For immunoblots *B* and *D*, densitometric ratios between phosphoprotein and total or loading control are provided. *Error bars*, S.E.

these defects are exacerbated by the addition of RLK deficiency, demonstrating the potential for combined inhibition (3). In NK cells, ITK functions as a positive regulator of the FcR pathway. FcR stimulation induces the tyrosine phosphorylation of ITK, leading to increases in granule release, calcium mobilization, and cytotoxicity (2). As expected, PRN694 potently blocked FcR activation and the effector functions of NK cells. The relative expression of ITK and RLK appears to be important for regulation of T helper cell differentiation as well (38). Specifically, Th1 cells express both ITK and RLK, whereas Th2 cells express only ITK. This is consistent with early studies with ITK knock-out mice that show that Th2- and IL-4-dependent disease processes, such as ovalbumin-induced asthma, are blocked by ITK deletion, whereas Th1 responses remain intact, presumably due to redundancy of RLK signaling (14, 48). RLK expression in Th17 cells is not well studied, but mice that have deletions of both kinases show profound defects in Th17 differentiation and function, a finding that was confirmed in our studies using human Th17 cells (9). Thus, combined inhibition of ITK and RLK would be expected to target both Th1 and Th17 cell differentiation and function. This could be an optimal therapeutic combination, given the importance of these two T helper cell subsets in the development of autoimmune diseases such as psoriasis, psoriatic arthritis, inflammatory bowel disease, and rheumatoid arthritis (49–56). Interestingly, recent data utilizing ITK knock-out mice indicate that along with the decrease in Th17 cell differentiation and function, there is an increase in Treg cells that function in suppres-

A

Time post dose	1hr	6hr	14hr
% ITK Occupancy	98.4 ± 0.6	95.4 ± 4.7	54.7 ± 15.4
Plasma PRN694 (μM)	2.8 ± 0.2μM	0.66 ± 0.01μM	0.027 ± 0.01μM

B

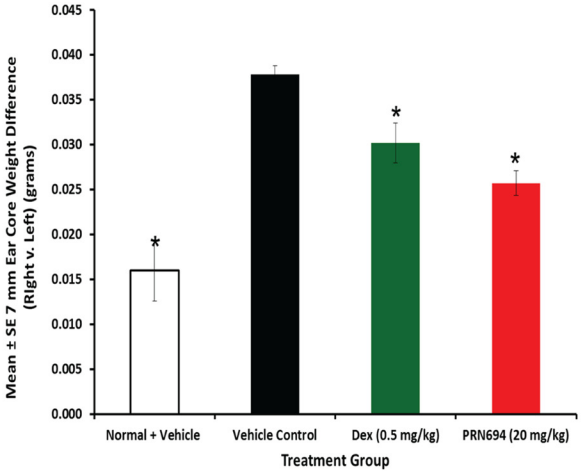

FIGURE 9. ***In vivo* pharmacokinetic and pharmacodynamic profile for PRN694 and *in vivo* inhibition of delayed type hypersensitivity in mice.** *A*, thymocytes were harvested from mice at the indicated time points following intraperitoneal administration of 20 mg/kg PRN694. The thymocytes were treated with an irreversible fluorescent probe for ITK to measure the target occupancy. After separation by SDS-PAGE, the amount of probe binding was measured by fluorescence scanning of the gel. Plasma was also harvested, and the concentration of PRN694 in the plasma was determined by mass spectrometry. *B*, mice were sensitized with oxazolone on the shaved abdomen and then 7 days later were challenged with oxazolone on both sides of the right ear or vehicle on both sides of the left ear. One hour prior to the challenges, mice were dosed intraperitoneally with vehicle, 0.5 mg/kg dexamethasone (positive control), or PRN694 (20 mg/kg). Twenty-four hours after the challenge, ear edema was measured by weighing 7-mm ear cores. *, $p < 0.05$. *Error bars*, S.E.

sion of disease in a murine adoptive transfer model of colitis (9). Thus, an added value of regulating the pathways targeted by PRN694 is potentially an increase in regulatory T-cells that also are important in control of autoimmune disease.

Although our studies reveal an NK cell dependence on RLK and ITK for FcR stimulation, this was not observed in monocyte-derived macrophages or dendritic cells. Moreover, our studies using the RBL-2H3 mast cell line demonstrated no effects of PRN694 on FcRϵ-induced activation, indicating that myeloid-derived immune cells are not uniquely dependent upon RLK and ITK. This concept is supported by recent literature indicating that BTK is a dominant regulator of mast cell FcRϵ degranulation and that ITK plays an accessory role, and only combined genetic ablation can eliminate degranulation (57). Notably, however, we did not observe significant expression of ITK in our RBL-2H3 cell line, indicating some potential molecular differences that warrant further study (58).

Medicinal chemistry discovery and optimization of ITK inhibitors have resulted in the identification of many chemical series with potent biochemical activities. However, due to the conserved topology and sequence composition of the ATP binding site of the TEC family and kinases in general, achieving high specificity has proven difficult (19, 59–62). A new chemical design strategy that can address the potency and selectivity challenges of kinase inhibition is based on covalent binding to cysteine residues within the ATP binding site. With the recent Food and Drug Administration approval of ibrutinib and the late stage development status of several other covalent kinase inhibitors, this approach is gaining widespread acceptance in the oncology arena (28, 63). Of primary importance for our novel approach was the identification a selective hinge-binding molecular scaffold and compatible linker chemistry to covalently bond to Cys-442. Although covalent ITK inhibitors targeting Cys-442 have been reported previously, there was limited success in achieving high selectivity (64). Cys-442 of ITK is located at the end of the C-lobe α-helix, a conserved location shared with only 10 other kinases, including all members of the TEC family (ITK, RLK, BTK, BMX, and TEC). As a consequence, a strategy to achieve high selectivity required more than simply targeting a covalent interaction with Cys-442. This approach optimizes the interactions with the targets of interest while limiting the interactions with off-target cysteine-containing proteins. Thus, small molecules with high potency, selectivity, and prolonged target residence time are produced, which may lead to superior safety and tolerability of clinical leads.

In addition to the potential utility for autoimmune diseases, our results support potential applications of PRN694 for the treatment of T-cell and NK cell-related cancers. Our *ex vivo* studies on T-PLL signaling demonstrate the potential for therapeutic utility for PRN694 in these hematopoietic malignan-

cies. Although the molecular pathogenesis of aggressive T-cell and NK cell malignancies remains unclear, ITK and RLK have been shown to be critical mediators of intracellular signaling that support the survival and growth of these malignancies (65–67). Our studies reveal that ITK- and RLK-based signaling in T-PLL can be blocked by PRN694, thereby starving these cells of an essential activation pathway. This effect is similar to how ibrutinib starves malignant leukemic B-cells by blocking BTK signaling. Further preclinical studies focusing on novel ITK- and/or RLK-relevant clinical applications for PRN694 are currently being pursued.

REFERENCES

1. Felices, M., and Berg, L. J. (2008) The Tec kinases Itk and Rlk regulate NKT cell maturation, cytokine production, and survival. *J. Immunol.* **180,** 3007–3018
2. Khurana, D., Arneson, L. N., Schoon, R. A., Dick, C. J., and Leibson, P. J. (2007) Differential regulation of human NK cell-mediated cytotoxicity by the tyrosine kinase Itk. *J. Immunol.* **178,** 3575–3582
3. Schaeffer, E. M., Debnath, J., Yap, G., McVicar, D., Liao, X. C., Littman, D. R., Sher, A., Varmus, H. E., Lenardo, M. J., and Schwartzberg, P. L. (1999) Requirement for Tec kinases Rlk and Itk in T cell receptor signaling and immunity. *Science* **284,** 638–641
4. Berg, L. J., Finkelstein, L. D., Lucas, J. A., and Schwartzberg, P. L. (2005) Tec family kinases in T lymphocyte development and function. *Annu. Rev. Immunol.* **23,** 549–600
5. Finkelstein, L. D., Shimizu, Y., and Schwartzberg, P. L. (2005) Tec kinases regulate TCR-mediated recruitment of signaling molecules and integrin-dependent cell adhesion. *J. Immunol.* **175,** 5923–5930
6. Readinger, J. A., Mueller, K. L., Venegas, A. M., Horai, R., and Schwartzberg, P. L. (2009) Tec kinases regulate T-lymphocyte development and function: new insights into the roles of Itk and Rlk/Txk. *Immunol. Rev.* **228,** 93–114
7. Fowell, D. J., Shinkai, K., Liao, X. C., Beebe, A. M., Coffman, R. L., Littman, D. R., and Locksley, R. M. (1999) Impaired NFATc translocation and failure of Th2 development in Itk-deficient $CD4^+$ T cells. *Immunity* **11,** 399–409
8. Mueller, C., and August, A. (2003) Attenuation of immunological symptoms of allergic asthma in mice lacking the tyrosine kinase ITK. *J. Immunol.* **170,** 5056–5063
9. Gomez-Rodriguez, J., Wohlfert, E. A., Handon, R., Meylan, F., Wu, J. Z., Anderson, S. M., Kirby, M. R., Belkaid, Y., and Schwartzberg, P. L. (2014) Itk-mediated integration of T cell receptor and cytokine signaling regulates the balance between Th17 and regulatory T cells. *J. Exp. Med.* **211,** 529–543
10. Papp, K. A., Leonardi, C., Menter, A., Ortonne, J. P., Krueger, J. G., Kricorian, G., Aras, G., Li, J., Russell, C. B., Thompson, E. H., and Baumgartner, S. (2012) Brodalumab, an anti-interleukin-17-receptor antibody for psoriasis. *N. Engl. J. Med.* **366,** 1181–1189
11. Waite, J. C., and Skokos, D. (2012) Th17 response and inflammatory autoimmune diseases. *Int. J. Inflam.* **2012,** 819467
12. Kannan, Y., and Wilson, M. S. (2012) TEC and MAPK kinase signalling pathways in T helper (T) cell development, T2 differentiation and allergic asthma. *J. Clin. Cell. Immunol.* **12,** 11
13. Gomez-Rodriguez, J., Sahu, N., Handon, R., Davidson, T. S., Anderson, S. M., Kirby, M. R., August, A., and Schwartzberg, P. L. (2009) Differential expression of interleukin-17A and -17F is coupled to T cell receptor signaling via inducible T cell kinase. *Immunity* **31,** 587–597
14. Ferrara, T. J., Mueller, C., Sahu, N., Ben-Jebria, A., and August, A. (2006) Reduced airway hyperresponsiveness and tracheal responses during allergic asthma in mice lacking tyrosine kinase inducible T-cell kinase. *J. Allergy Clin. Immunol.* **117,** 780–786
15. Vargas, L., Hamasy, A., Nore, B. F., and Smith, C. I. (2013) Inhibitors of BTK and ITK: state of the new drugs for cancer, autoimmunity and inflammatory diseases. *Scand. J. Immunol.* **78,** 130–139
16. Warner, K., Crispatzu, G., Al-Ghaili, N., Weit, N., Florou, V., You, M. J., Newrzela, S., and Herling, M. (2013) Models for mature T-cell lymphomas: a critical appraisal of experimental systems and their contribution to current T-cell tumorigenic concepts. *Crit. Rev. Oncol. Hematol.* **88,** 680–695
17. Warner, K., Weit, N., Crispatzu, G., Admirand, J., Jones, D., and Herling, M. (2013) T-cell receptor signaling in peripheral T-cell lymphoma: a review of patterns of alterations in a central growth regulatory pathway. *Curr. Hematol. Malig. Rep.* **8,** 163–172
18. Alder, C. M., Ambler, M., Campbell, A. J., Champigny, A. C., Deakin, A. M., Harling, J. D., Harris, C. A., Longstaff, T., Lynn, S., Maxwell, A. C., Mooney, C. J., Scullion, C., Singh, O. M., Smith, I. E., Somers, D. O., Tame, C. J., Wayne, G., Wilson, C., and Woolven, J. M. (2013) Identification of a novel and selective series of Itk inhibitors via a template-hopping strategy. *ACS Med. Chem. Lett.* **4,** 948–952
19. Charrier, J. D., Miller, A., Kay, D. P., Brenchley, G., Twin, H. C., Collier, P. N., Ramaya, S., Keily, S. B., Durrant, S. J., Knegtel, R. M., Tanner, A. J., Brown, K., Curnock, A. P., and Jimenez, J. M. (2011) Discovery and structure-activity relationship of 3-aminopyrid-2-ones as potent and selective interleukin-2 inducible T-cell kinase (Itk) inhibitors. *J. Med. Chem.* **54,** 2341–2350
20. McLean, L. R., Zhang, Y., Zaidi, N., Bi, X., Wang, R., Dharanipragada, R., Jurcak, J. G., Gillespy, T. A., Zhao, Z., Musick, K. Y., Choi, Y. M., Barrague, M., Peppard, J., Smicker, M., Duguid, M., Parkar, A., Fordham, J., and Kominos, D. (2012) X-ray crystallographic structure-based design of selective thienopyrazole inhibitors for interleukin-2-inducible tyrosine kinase. *Bioorg. Med. Chem. Lett.* **22,** 3296–3300
21. Pastor, R. M., Burch, J. D., Magnuson, S., Ortwine, D. F., Chen, Y., De La Torre, K., Ding, X., Eigenbrot, C., Johnson, A., Liimatta, M., Liu, Y., Shia, S., Wang, X., Wu, L. C., and Pei, Z. (2014) Discovery and optimization of indazoles as potent and selective interleukin-2 inducible T cell kinase (ITK) inhibitors. *Bioorg. Med. Chem. Lett.* **24,** 2448–2452
22. Moriarty, K. J., Takahashi, H., Pullen, S. S., Khine, H. H., Sallati, R. H., Raymond, E. L., Woska, J. R., Jr., Jeanfavre, D. D., Roth, G. P., Winters, M. P., Qiao, L., Ryan, D., DesJarlais, R., Robinson, D., Wilson, M., Bobko, M., Cook, B. N., Lo, H. Y., Nemoto, P. A., Kashem, M. A., Wolak, J. P., White, A., Magolda, R. L., and Tomczuk, B. (2008) Discovery, SAR and x-ray structure of 1H-benzimidazole-5-carboxylic acid cyclohexyl-methyl-amides as inhibitors of inducible T-cell kinase (Itk). *Bioorg. Med. Chem. Lett.* **18,** 5545–5549
23. Han, S., Czerwinski, R. M., Caspers, N. L., Limburg, D. C., Ding, W., Wang, H., Ohren, J. F., Rajamohan, F., McLellan, T. J., Unwalla, R., Choi, C., Parikh, M. D., Seth, N., Edmonds, J., Phillips, C., Shakya, S., Li, X., Spaulding, V., Hughes, S., Cook, A., Robinson, C., Mathias, J. P., Navratilova, I., Medley, Q. G., Anderson, D. R., Kurumbail, R. G., and Aulabaugh, A. (2014) Selectively targeting an inactive conformation of interleukin-2-inducible T-cell kinase by allosteric inhibitors. *Biochem. J.* **460,** 211–222
24. Carpenter, R. L., and Lo, H. W. (2012) Dacomitinib, an emerging HER-targeted therapy for non-small cell lung cancer. *J. Thorac. Dis.* **4,** 639–642
25. Serafimova, I. M., Pufall, M. A., Krishnan, S., Duda, K., Cohen, M. S., Maglathlin, R. L., McFarland, J. M., Miller, R. M., Frödin, M., and Taunton, J. (2012) Reversible targeting of noncatalytic cysteines with chemically tuned electrophiles. *Nat. Chem. Biol.* **8,** 471–476
26. Byrd, J. C., Furman, R. R., Coutre, S. E., Flinn, I. W., Burger, J. A., Blum, K. A., Grant, B., Sharman, J. P., Coleman, M., Wierda, W. G., Jones, J. A., Zhao, W., Heerema, N. A., Johnson, A. J., Sukbuntherng, J., Chang, B. Y., Clow, F., Hedrick, E., Buggy, J. J., James, D. F., and O'Brien, S. (2013) Targeting BTK with ibrutinib in relapsed chronic lymphocytic leukemia. *N. Engl. J. Med.* **369,** 32–42
27. Wang, M. L., Rule, S., Martin, P., Goy, A., Auer, R., Kahl, B. S., Jurczak, W., Advani, R. H., Romaguera, J. E., Williams, M. E., Barrientos, J. C., Chmielowska, E., Radford, J., Stilgenbauer, S., Dreyling, M., Jedrzejczak, W. W., Johnson, P., Spurgeon, S. E., Li, L., Zhang, L., Newberry, K., Ou, Z., Cheng, N., Fang, B., McGreivy, J., Clow, F., Buggy, J. J., Chang, B. Y., Beaupre, D. M., Kunkel, L. A., and Blum, K. A. (2013) Targeting BTK with ibrutinib in relapsed or refractory mantle-cell lymphoma. *N. Engl. J. Med.* **369,** 507–516
28. Dubovsky, J. A., Beckwith, K. A., Natarajan, G., Woyach, J. A., Jaglowski, S., Zhong, Y., Hessler, J. D., Liu, T. M., Chang, B. Y., Larkin, K. M., Ste-

fanovski, M. R., Chappell, D. L., Frissora, F. W., Smith, L. L., Smucker, K. A., Flynn, J. M., Jones, J. A., Andritsos, L. A., Maddocks, K., Lehman, A. M., Furman, R., Sharman, J., Mishra, A., Caligiuri, M. A., Satoskar, A. R., Buggy, J. J., Muthusamy, N., Johnson, A. J., and Byrd, J. C. (2013) Ibrutinib is an irreversible molecular inhibitor of ITK driving a Th1 selective pressure in T-lymphocytes. *Blood* **122,** 2539–2549

29. Pfaffl, M. W. (2001) A new mathematical model for relative quantification in real-time RT-PCR. *Nucleic Acids Res.* **29,** e45
30. Dubovsky, J. A., McNeel, D. G., Powers, J. J., Gordon, J., Sotomayor, E. M., and Pinilla-Ibarz, J. A. (2009) Treatment of chronic lymphocytic leukemia with a hypomethylating agent induces expression of NXF2, an immunogenic cancer testis antigen. *Clin. Cancer Res.* **15,** 3406–3415
31. Wu, L., Adams, M., Carter, T., Chen, R., Muller, G., Stirling, D., Schafer, P., and Bartlett, J. B. (2008) Lenalidomide enhances natural killer cell and monocyte-mediated antibody-dependent cellular cytotoxicity of rituximab-treated $CD20^+$ tumor cells. *Clin. Cancer Res.* **14,** 4650–4657
32. Zhong, Y., Sullenbarger, B., and Lasky, L. C. (2010) Effect of increased HoxB4 on human megakaryocytic development. *Biochem. Biophys. Res. Commun.* **398,** 377–382
33. Susaki, K., Kitanaka, A., Dobashi, H., Kubota, Y., Kittaka, K., Kameda, T., Yamaoka, G., Mano, H., Mihara, K., and Ishida, T. (2010) Tec protein tyrosine kinase inhibits CD25 expression in human T-lymphocyte. *Immunol. Lett.* **127,** 135–142
34. Bergamini, G., Bell, K., Shimamura, S., Werner, T., Cansfield, A., Müller, K., Perrin, J., Rau, C., Ellard, K., Hopf, C., Doce, C., Leggate, D., Mangano, R., Mathieson, T., O'Mahony, A., Plavec, I., Rharbaoui, F., Reinhard, F., Savitski, M. M., Ramsden, N., Hirsch, E., Drewes, G., Rausch, O., Bantscheff, M., and Neubauer, G. (2012) A selective inhibitor reveals PI3Kγ dependence of T(H)17 cell differentiation. *Nat. Chem. Biol.* **8,** 576–582
35. Melton, A. C., Melrose, J., Alajoki, L., Privat, S., Cho, H., Brown, N., Plavec, A. M., Nguyen, D., Johnston, E. D., Yang, J., Polokoff, M. A., Plavec, I., Berg, E. L., and O'Mahony, A. (2013) Regulation of IL-17A production is distinct from IL-17F in a primary human cell co-culture model of T cell-mediated B cell activation. *PLoS One* **8,** e58966
36. Xu, D., Kim, Y., Postelnek, J., Vu, M. D., Hu, D. Q., Liao, C., Bradshaw, M., Hsu, J., Zhang, J., Pashine, A., Srinivasan, D., Woods, J., Levin, A., O'Mahony, A., Owens, T. D., Lou, Y., Hill, R. J., Narula, S., DeMartino, J., and Fine, J. S. (2012) RN486, a selective Bruton's tyrosine kinase inhibitor, abrogates immune hypersensitivity responses and arthritis in rodents. *J. Pharmacol. Exp. Ther.* **341,** 90–103
37. Lin, T. A., McIntyre, K. W., Das, J., Liu, C., O'Day, K. D., Penhallow, B., Hung, C. Y., Whitney, G. S., Shuster, D. J., Yang, X., Townsend, R., Postelnek, J., Spergel, S. H., Lin, J., Moquin, R. V., Furch, J. A., Kamath, A. V., Zhang, H., Marathe, P. H., Perez-Villar, J. J., Doweyko, A., Killar, L., Dodd, J. H., Barrish, J. C., Wityak, J., and Kanner, S. B. (2004) Selective Itk inhibitors block T-cell activation and murine lung inflammation. *Biochemistry* **43,** 11056–11062
38. Andreotti, A. H., Schwartzberg, P. L., Joseph, R. E., and Berg, L. J. (2010) T-cell signaling regulated by the Tec family kinase, Itk. *Cold Spring Harb. Perspect. Biol.* **2,** a002287
39. Alter, G., Malenfant, J. M., and Altfeld, M. (2004) CD107a as a functional marker for the identification of natural killer cell activity. *J. Immunol. Methods* **294,** 15–22
40. Cohnen, A., Chiang, S. C., Stojanovic, A., Schmidt, H., Claus, M., Saftig, P., Janssen, O., Cerwenka, A., Bryceson, Y. T., and Watzl, C. (2013) Surface CD107a/LAMP-1 protects natural killer cells from degranulation-associated damage. *Blood* **122,** 1411–1418
41. Köprülü, A. D., Kastner, R., Wienerroither, S., Lassnig, C., Putz, E. M., Majer, O., Reutterer, B., Sexl, V., Kuchler, K., Müller, M., Decker, T., and Ellmeier, W. (2013) The tyrosine kinase Btk regulates the macrophage response to *Listeria monocytogenes* infection. *PLoS One* **8,** e60476
42. Kosaka, Y., Felices, M., and Berg, L. J. (2006) Itk and Th2 responses: action but no reaction. *Trends Immunol.* **27,** 453–460
43. Horwood, N. J., Urbaniak, A. M., and Danks, L. (2012) Tec family kinases in inflammation and disease. *Int. Rev. Immunol.* **31,** 87–103
44. Bedoya, S. K., Lam, B., Lau, K., and Larkin, J., 3rd (2013) Th17 cells in immunity and autoimmunity. *Clin. Dev. Immunol.* **2013,** 986789
45. Galli, S. J., and Hammel, I. (1984) Unequivocal delayed hypersensitivity in mast cell-deficient and beige mice. *Science* **226,** 710–713
46. Liao, X. C., and Littman, D. R. (1995) Altered T cell receptor signaling and disrupted T cell development in mice lacking Itk. *Immunity* **3,** 757–769
47. Liu, K. Q., Bunnell, S. C., Gurniak, C. B., and Berg, L. J. (1998) T cell receptor-initiated calcium release is uncoupled from capacitative calcium entry in Itk-deficient T cells. *J. Exp. Med.* **187,** 1721–1727
48. Sahu, N., and August, A. (2009) ITK inhibitors in inflammation and immune-mediated disorders. *Curr. Top. Med. Chem.* **9,** 690–703
49. Lowes, M. A., Kikuchi, T., Fuentes-Duculan, J., Cardinale, I., Zaba, L. C., Haider, A. S., Bowman, E. P., and Krueger, J. G. (2008) Psoriasis vulgaris lesions contain discrete populations of Th1 and Th17 T cells. *J. Invest. Dermatol.* **128,** 1207–1211
50. Uyemura, K., Yamamura, M., Fivenson, D. F., Modlin, R. L., and Nickoloff, B. J. (1993) The cytokine network in lesional and lesion-free psoriatic skin is characterized by a T-helper type 1 cell-mediated response. *J. Invest. Dermatol.* **101,** 701–705
51. Zaba, L. C., Fuentes-Duculan, J., Eungdamrong, N. J., Abello, M. V., Novitskaya, I., Pierson, K. C., Gonzalez, J., Krueger, J. G., and Lowes, M. A. (2009) Psoriasis is characterized by accumulation of immunostimulatory and Th1/Th17 cell-polarizing myeloid dendritic cells. *J. Invest. Dermatol.* **129,** 79–88
52. Kobayashi, T., Okamoto, S., Hisamatsu, T., Kamada, N., Chinen, H., Saito, R., Kitazume, M. T., Nakazawa, A., Sugita, A., Koganei, K., Isobe, K., and Hibi, T. (2008) IL23 differentially regulates the Th1/Th17 balance in ulcerative colitis and Crohn's disease. *Gut* **57,** 1682–1689
53. Hundorfean, G., Neurath, M. F., and Mudter, J. (2012) Functional relevance of T helper 17 (Th17) cells and the IL-17 cytokine family in inflammatory bowel disease. *Inflamm. Bowel Dis.* **18,** 180–186
54. Brand, S. (2009) Crohn's disease: Th1, Th17 or both? The change of a paradigm: new immunological and genetic insights implicate Th17 cells in the pathogenesis of Crohn's disease. *Gut* **58,** 1152–1167
55. Shen, H., Goodall, J. C., and Hill Gaston, J. S. (2009) Frequency and phenotype of peripheral blood Th17 cells in ankylosing spondylitis and rheumatoid arthritis. *Arthritis Rheum.* **60,** 1647–1656
56. Hirota, K., Yoshitomi, H., Hashimoto, M., Maeda, S., Teradaira, S., Sugimoto, N., Yamaguchi, T., Nomura, T., Ito, H., Nakamura, T., Sakaguchi, N., and Sakaguchi, S. (2007) Preferential recruitment of CCR6-expressing Th17 cells to inflamed joints via CCL20 in rheumatoid arthritis and its animal model. *J. Exp. Med.* **204,** 2803–2812
57. Iyer, A. S., Morales, J. L., Huang, W., Ojo, F., Ning, G., Wills, E., Baines, J. D., and August, A. (2011) Absence of Tec family kinases interleukin-2 inducible T cell kinase (Itk) and Bruton's tyrosine kinase (Btk) severely impairs FcεRI-dependent mast cell responses. *J. Biol. Chem.* **286,** 9503–9513
58. Kawakami, Y., Yao, L., Tashiro, M., Gibson, S., Mills, G. B., and Kawakami, T. (1995) Activation and interaction with protein kinase C of a cytoplasmic tyrosine kinase, Itk/Tsk/Emt, on FcεRI cross-linking on mast cells. *J. Immunol.* **155,** 3556–3562
59. Das, J., Furch, J. A., Liu, C., Moquin, R. V., Lin, J., Spergel, S. H., McIntyre, K. W., Shuster, D. J., O'Day, K. D., Penhallow, B., Hung, C. Y., Doweyko, A. M., Kamath, A., Zhang, H., Marathe, P., Kanner, S. B., Lin, T. A., Dodd, J. H., Barrish, J. C., and Wityak, J. (2006) Discovery and SAR of 2-amino-5-(thioaryl)thiazoles as potent and selective Itk inhibitors. *Bioorg. Med. Chem. Lett.* **16,** 3706–3712
60. Guo, W., Liu, R., Ono, Y., Ma, A. H., Martinez, A., Sanchez, E., Wang, Y., Huang, W., Mazloom, A., Li, J., Ning, J., Maverakis, E., Lam, K. S., and Kung, H. J. (2012) Molecular characteristics of CTA056, a novel interleukin-2-inducible T-cell kinase inhibitor that selectively targets malignant T cells and modulates oncomirs. *Mol. Pharmacol.* **82,** 938–947
61. Snow, R. J., Abeywardane, A., Campbell, S., Lord, J., Kashem, M. A., Khine, H. H., King, J., Kowalski, J. A., Pullen, S. S., Roma, T., Roth, G. P., Sarko, C. R., Wilson, N. S., Winters, M. P., Wolak, J. P., and Cywin, C. L. (2007) Hit-to-lead studies on benzimidazole inhibitors of ITK: discovery of a novel class of kinase inhibitors. *Bioorg. Med. Chem. Lett.* **17,** 3660–3665
62. Velankar, A. D., Quintini, G., Prabhu, A., Weber, A., Hunaeus, G., Voland, B., Wuest, M., Orjeda, C., Harel, D., Varghese, S., Gore, V., Patil, M., Gayke, D., Herdemann, M., Heit, I., and Zaliani, A. (2010) Synthesis and

biological evaluation of novel (4 or 5-aryl)pyrazolyl-indoles as inhibitors of interleukin-2 inducible T-cell kinase (ITK). *Bioorg. Med. Chem.* **18,** 4547–4559

63. Pan, Z., Scheerens, H., Li, S. J., Schultz, B. E., Sprengeler, P. A., Burrill, L. C., Mendonca, R. V., Sweeney, M. D., Scott, K. C., Grothaus, P. G., Jeffery, D. A., Spoerke, J. M., Honigberg, L. A., Young, P. R., Dalrymple, S. A., and Palmer, J. T. (2007) Discovery of selective irreversible inhibitors for Bruton's tyrosine kinase. *Chem. Med. Chem.* **2,** 58–61
64. Harling, J. D., Deakin, A. M., Campos, S., Grimley, R., Chaudry, L., Nye, C., Polyakova, O., Bessant, C. M., Barton, N., Somers, D., Barrett, J., Graves, R. H., Hanns, L., Kerr, W. J., and Solari, R. (2013) Discovery of novel irreversible inhibitors of interleukin (IL)-2-inducible tyrosine kinase (Itk) by targeting cysteine 442 in the ATP pocket. *J. Biol. Chem.* **288,** 28195–28206
65. Kaukonen, J., Savolainen, E. R., and Palotie, A. (1999) Human Emt tyrosine kinase is specifically expressed both in mature T-lymphocytes and T-cell associated hematopoietic malignancies. *Leuk. Lymphoma* **32,** 513–522
66. Shin, J., Monti, S., Aires, D. J., Duvic, M., Golub, T., Jones, D. A., and Kupper, T. S. (2007) Lesional gene expression profiling in cutaneous T-cell lymphoma reveals natural clusters associated with disease outcome. *Blood* **110,** 3015–3027
67. Zhao, W. L. (2010) Targeted therapy in T-cell malignancies: dysregulation of the cellular signaling pathways. *Leukemia* **24,** 13–21
68. Brameld, K. A., and Owens, T. A. (March 6, 2014) International Patent WO 2014/036016 A1